Title
Development of Cell and Gene Therapies for the Treatment of Carbamoyl Phosphate Synthetase 1 Deficiency

Author
Nitzahn, Matthew

Publication Date
2021

Peer reviewed|Thesis/dissertation

UNIVERSITY OF CALIFORNIA

Los Angeles

Development of Cell and Gene Therapies for the Treatment of Carbamoyl Phosphate Synthetase 1 Deficiency

A dissertation submitted in partial satisfaction of the requirements

for the degree Doctor of Philosophy in Molecular Biology

by

Matthew David Nitzahn

2021

ABSTRACT OF THE DISSERTATION

Development of Cell and Gene Therapies for the Treatment of

Carbamoyl Phosphate Synthetase 1 Deficiency

by

Matthew David Nitzahn

Doctor of Philosophy in Molecular Biology

University of California, Los Angeles, 2021

Professor Gerald S. Lipshutz, Chair

The urea cycle is essential in terrestrial mammals to detoxify ammonia into urea, and disruptions of this process may lead to neurotoxic ammonia levels and growth deficits. Carbamoyl phosphate synthetase 1 (CPS1) deficiency is caused by a loss of functional CPS1 protein, which catalyzes the initial and rate-limiting step of the urea cycle. Protein-restricted diets and chronic use of ammonia scavengers, the standards of care, are only modestly effective for treating CPS1 deficiency. The only curative option is orthotopic liver transplantation, which is limited by low donor availability and complications from surgery/immunosuppression. To investigate and develop novel therapeutics, we took two separate but converging approaches using either cell- or

virus-based approaches. The first approach was to establish induced pluripotent stem cell lines from patients and use them as a platform to test potentially therapeutic genome modifications using the CRISPR/Cas9 system. Genomic addition of human codon optimized CPS1 (hcoCPS1) at the adeno-associated virus (AAV) insertion site, a known euchromatic safe harbor for exogenous genes, failed to reconstitute ureagenesis, demonstrating that further work is needed to improve and optimize this approach. The second approach utilized a split AAV platform to deliver hcoCPS1 to Cps1 deficient mice. hcoCPS1, along with its regulatory elements, is too large to fit into a single AAV capsid; by splitting the entire transgenic cassette in two, we capitalized on the recombinogenic nature of AAVs to reconstitute the full-length transgene *in vivo* and restore urea production. This approach successfully prevented mortality and reestablished ureagenesis in Cps1 deficient mice. The studies here provide the first insights into clinically translatable gene and cell therapies for CPS1 deficiency patients who have had no access to new treatments for over 40 years.

The dissertation of Matthew David Nitzahn is approved.

April D. Pyle

Lily Wu

David S. Williams

Wayne W. Grody

Gerald S. Lipshutz, Committee Chair

University of California, Los Angeles

2021

DEDICATION

To my parents, who believed in me unwaveringly from the beginning; and to my mentor, Gerry, who took a chance on me and provided the guidance I needed to flourish.

TABLE OF CONTENTS

Abstract of the Dissertation ……..……...ii

Committee …….…….....iv

Dedication ..……..…….……..……v

Table of Contents ……...vi

List of Figures and Tables ……vii

Acknowledgements……..viii

Vita……..……...ix

Chapter 1: Introduction……..……..…1

Chapter 2: CRISPR-Mediated Genomic Addition to CPS1 Deficient iPSCs

Is Insufficient to Restore Nitrogen Homeostasis…….…8

Chapter 3: Split AAV-Mediated Gene Therapy Restores Ureagenesis in a Murine

Model of Carbamoyl Phosphate Synthetase 1 Deficiency…….……..…..…..34

Chapter 4: Summary and Concluding Remarks……...……..71

References …….……77

LIST OF FIGURES AND TABLES

Chapter 1

Figure 1-1: Diagram of the mammalian urea cycle ……..……..…7

Chapter 2

Figure 2-1: Characterization of patient-derived iPSCs ……....….25

Figure 2-2: Design and validation of CRISPR/Cas9 editing in iPSCs at the *AAVS1* locus ……..27

Figure 2-3: Differentiation of iPSCs to HLCs ……....28

Figure 2-4: Investigating the factors contributing to differential ammonia metabolism in unedited and edited HLCs ……..……..……..….30

Table 2-1: Primers list ……..……..…32

Chapter 3

Figure 3-1: *In Vitro* Characterization of sAAVs ……..….58

Figure 3-2: sAAVs Promote Lifespan Extension and Weight Maintenance in Mice *In Vivo* …...60

Figure 3-3: sAAV Treatment Improves Some Amino Acid Imbalances in Mice with Cps1 Deficiency ……...63

Figure 3-4: Ammonia metabolism after exogenous ammonia loading ……..….65

Figure 3-5: Molecular analysis of livers from treated mice ……..…..67

Table 3-1: Ammonia challenge behavioral scores ……....68

Table 3-2: List of primers ……....69

ACKNOWLEDGEMENTS

Chapter 1 is adapted from Nitzahn, M., and Lipshutz, G.S. (2020). CPS1: Looking at an ancient enzyme in a modern light. Molecular Genetics and Metabolism 131, 289–298.

Chapter 2 is adapted from a manuscript currently in submission. Nitzahn, M., Truong, B., Khoja, S., Vega-Crespo, A., Le, C., Eliav, A., Makris, G., Pyle, A.D., Häberle, J., Lipshutz, G.S. CRISPR-Mediated Genomic Addition to CPS1 Deficient iPSCs Is Insufficient to Restore Nitrogen Homeostasis.

Chapter 3 is adapted from Nitzahn, M., Allegri, G., Khoja, S., Truong, B., Makris, G., Häberle, J., Lipshutz, G.S. (2020). Split AAV-Mediated Gene Therapy Restores Ureagenesis in a Murine Model of Carbamoyl Phosphate Synthetase 1 Deficiency. Molecular Therapy 28, 1717–1730.

In addition to co-authors in the above-referenced works, several others contributed in non-scientific capacities, including Joan Warner, without whom working in the lab would have been impossible, and the MBIDP student affairs officers Stephanie Cuellar and Ashley TerHorst, who were delightful to work with on administrative tasks both great and small.

This work was supported by National Institute of Neurological Disorders and Stroke grant R21NS091654, as well as the Philip Whitcome Pre-Doctoral Fellowship at UCLA.

VITA

EDUCATION

2013	Bachelor of Science, University of California, Los Angeles
	Molecular, Cell, and Developmental Biology

HONORS AND AWARDS

2018 – 2020	Philip Whitcome Pre-Doctoral Fellowship in Molecular Biology
	University of California, Los Angeles
2019	Meritorious Abstract Travel Award
	American Society of Gene and Cell Therapy, 22nd Annual Conference
2016 – 2017	Ruth L. Kirschstein National Research Service Award Institutional Research Training Grant Fellow in Vascular Biology
	University of California, Los Angeles
2009 – 2012	Dean's List Scholar Award
	Los Angeles Community College District and
	University of California, Los Angeles
2011	Scholar-Athlete Award
	Los Angeles Valley College

PUBLICATIONS

1. **Nitzahn, M.**, and Lipshutz, G.S. (2020). CPS1: Looking at an ancient enzyme in a modern light. Molecular Genetics and Metabolism *131*, 289–298.

2. **Nitzahn, M**., Allegri, G., Khoja, S., Truong, B., Makris, G., Häberle, J., and Lipshutz, G.S. (2020). Split AAV-Mediated Gene Therapy Restores Ureagenesis in a Murine Model of Carbamoyl Phosphate Synthetase 1 Deficiency. Molecular Therapy *28*, 1717–1730.
3. Soria, L.R., **Nitzahn, M**., Angelis, A.D., Khoja, S., Attanasio, S., Annunziata, P., Palmer, D.J., Ng, P., Lipshutz, G.S., and Brunetti-Pierri, N. (2019). Hepatic glutamine synthetase augmentation enhances ammonia detoxification. Journal of Inherited Metabolic Disease *42*, 1128–1135.
4. Khoja, S.*, **Nitzahn, M.***, Truong, B., Lambert, J., Willis, B., Allegri, G., Rüfenacht, V., Häberle, J., and Lipshutz, G.S. (2019). A constitutive knockout of murine carbamoyl phosphate synthetase 1 results in death with marked hyperglutaminemia and hyperammonemia. Journal of Inherited Metabolic Disease *42*, 1044–1053. *****Contributed equally
5. Khoja, S., **Nitzahn, M**., Hermann, K., Truong, B., Borzone, R., Willis, B., Rudd, M., Palmer, D.J., Ng, P., Brunetti-Pierri, N., et al. (2018). Conditional disruption of hepatic carbamoyl phosphate synthetase 1 in mice results in hyperammonemia without orotic aciduria and can be corrected by liver-directed gene therapy. Molecular Genetics and Metabolism *124*, 243–253.
6. Angarita, S.A.K., Truong, B., Khoja, S., **Nitzahn, M**., Rajbhandari, A.K., Zhuravka, I., Duarte, S., Lin, M.G., Lam, A.K., Cederbaum, S.D., et al. (2018). Human hepatocyte transplantation corrects the inherited metabolic liver disorder arginase deficiency in mice. Molecular Genetics and Metabolism *124*, 114–123.

Chapter 1: Introduction

In ureotelic animals, nitrogen produced as a byproduct of amino acid catabolism is detoxified in the liver by the urea cycle, a system of 5 (6 including n-acetylglutamate synthase [NAGS]) enzymes and two transporter proteins (Figure 1-1). Partial or total loss of function in any of the urea cycle proteins results in urea cycle disorders (UCDs), which occur in 1:35,000[1,2] to 1:50,000[3,4] live births. The first enzyme in the cycle is carbamoyl phosphate synthetase 1 (CPS1; E.C. 6.3.4.16), which catalyzes the ATP-dependent condensation of bicarbonate and ammonia to form carbamoyl phosphate[5]. Carbamoyl phosphate undergoes stepwise catalysis to eventually form urea, which is released into the blood for excretion by the kidneys. CPS1 deficiency (OMIM #237300) is an autosomal recessive disorder[6] with a prevalence of 1 in 300,000[2] to 1 in 1.3 million births[1]; estimates vary widely due to difficulty in diagnosis. Patients typically present with lethargy, vomiting, encephalopathy, and coma; subsequent blood analysis typically demonstrates elevated ammonia and glutamine along with reduced citrulline and arginine[7]. While the majority of cases appear in the neonatal period, others present less frequently, occurring any time from childhood to adulthood depending on the extent of CPS1 functional loss. In neonates, up to 50% of symptomatic patients perish despite treatment[2], many with the first episode of hyperammonemia; late-onset patients have survival of over 90%[8]. Long-term neurological deficits are found in the vast majority of neonatal onset cases, with a smaller proportion occurring in those diagnosed as late-onset[4].

Clinical management of CPS1 deficiency is largely dependent on dietary protein restriction, administration of the nitrogen scavenging compounds phenylbutyrate and benzoate[9,10], and L-arginine supplementation[11]. Keto analogues of amino acids (e.g. valine or phenylalanine) have also been used successfully[12]. However, these therapies are unable to prevent progressive neurological decline due to recurrent hyperammonemia, which often requires emergent

hemodialysis to effectively clear[13]. Dialysis is effective in preventing mortality in some severe cases but ultimately is unable to improve neurocognitive outcomes. Nitrogen scavengers are further limited by toxicity at high doses and unwanted side effects from chronic use[14–16]. Early diagnosis and aggressive treatment are therefore essential for improving prognoses; however, initial diagnosis is hindered by the lack of a specific metabolite that distinguishes it from NAGS deficiency[17], necessitating genome sequencing or functional testing. Pre-natal and newborn screening could have a meaningful impact in speeding up diagnosis, though it is not routinely performed for CPS1[18]. These difficulties are exacerbated by the fact that CPS1 deficient patients tend to have the most severe symptoms of all UCDs[2]. Orthotopic liver transplantation is effective in treating deficiency of CPS1[19,20], though there are potential associated complications including allograft rejection and post-operative infections[21]. In addition, despite the high level of survival post-surgery[22], patients require long-term immunosuppression and may still require citrulline supplementation due to loss of CPS1 activity in enterocytes, the primary source of plasma citrulline[7,20].

Novel therapies are therefore needed to treat CPS1 deficient patients that reduce or eliminate reliance on liver transplantation. One intriguing potential alternative to full liver transplantation is hepatocyte transplantation. Though this strategy retains the immune suppression drawback, it has the advantage of being less invasive with lower risk for peri- and post-operative complications. This approach can also amplify the number of patients treated with cells from a single donor, reducing demand for donor organs. Though hepatocyte transplantation has been used successfully to treat CPS1 deficiency in limited cases[23], healthy hepatocytes for transplantation are still in short supply, making alternate cell sources more desirable. Both embryonic and patient-derived induced pluripotent stem cells (iPSCs) can develop into any cell type[24], including

hepatocytes, with several and ever-improving strategies for liver-specific differentiation currently available[25–29]. They may therefore represent an unlimited supply of hepatic cells for transplantation. With the widespread usage and application of iPSCs for regenerative medicine[30–32], hepatocytes generated *in vitro* from patient cells have the potential to address donor organ shortages and immunosuppression hurdles in a single technology.

To make patient iPSC-derived hepatocytes ready for transplantation, the offending genetic mutations must first be either corrected or bypassed. Zinc finger and transcription activator–like effector nucleases (ZFNs and TALENs, respectively) are similar platforms for genome editing involving the fusion of a DNA endonuclease to a customizable DNA binding protein[33,34]. While useful for making targeted modifications, both ZFN and TALEN technologies are limited by the necessary dimerization of the endonuclease to function, meaning that two separate proteins must be designed and co-expressed[35]. The clustered regularly interspaced short palindromic repeats (CRISPR)/Cas9 system has emerged over the past decade as the tool of choice for rapid and accurate genome editing. After its initial discovery and usage in mammalian cells[36,37], CRISPR/Cas9 has been used to successfully edit multiple cell types, including iPSCs[38]. In this system, a single guide RNA directs the Cas9 protein to one specific location on genomic DNA that is complementary to the RNA, where Cas9 then induces a double-strand break. By supplying an exogenous donor sequence of interest, the native homology-dependent repair mechanisms of the cell can use that donor to incorporate the desired changes in a site-specific fashion. The CRISPR/Cas9 platform is more rapid and less labor intensive than previous ZFNs and TALENs[39] because a universal Cas9 protein may be paired with different guide RNAs that are relatively simple to design bioinformatically, making it ideal for use in tandem with iPSC technology.

While stem cell-based treatments may provide an alternative to liver transplantation, they are currently limited somewhat in their capacity due to generally poor engraftment in the host liver[40–42]. Advances in artificial livers generated on scaffolds[43] could address this limitation but require additional time to produce with concomitant increased cost. A virus-based gene therapy approach could potentially circumvent these issues. Classic virus-mediated gene therapies throughout the 1990s and early 2000s were heavily focused on using retro-, lenti-, and adenoviruses. However, the risks of insertional mutagenesis (retro- and lentiviruses)[44] and immunogenicity (adenoviruses)[45], which led to the death of a patient[46], necessitate the use of alternative viruses. In particular, adeno-associated viruses (AAVs) have recently shown great therapeutic promise in both pre-clinical[47] and clinical[48] contexts due to their reduced propensity for genomic insertion, high titers in production, and low immunogenicity (reviewed in Colella *et al.* 2018)[49]. Successful investigations into their use to treat other metabolic disorders[50], including those of the urea cycle[51,52], highlight their therapeutic potential for treating CPS1 deficiency.

The recent development of several model systems has led to the ability to test and develop novel treatments for CPS1 deficiency. For the majority of the past 60 years, biochemical studies relied on isolating CPS1 from model organisms such as *E. coli* and rats, leaving the clinical impact of various described human mutations uncharacterized. Recently, several updated cell models have been established, including those based on *E. coli*[53], insect[54,55], yeast[56], and human[57,58] cells to express recombinant CPS1 to specifically investigate the impacts of clinically relevant mutations. While these models provide key insights into purified enzyme function and kinetics, they are incapable of providing a platform with which to develop treatments. To design and test potential therapeutics, robust animal models are essential; however, the severity of disease symptoms and high therapeutic threshold have made the development of animal models technically

challenging[59,60]. To address the need for new models, we recently generated and characterized two models of CPS1 deficiency in mice. In the constitutive knock out, neonates homozygous for a deletion in exons 3 and 4 rapidly develop lethal hyperammonemia with milk intake and perish within 24 hours of birth[61]. This model recapitulates the severe neonatal human phenotype as well as a previously published model also describing a constitutive knock out[62], though this original mouse line has since been lost[63]. We also generated a conditional knock out mouse model that uses the Cre/LoxP system to delete exons 3 and 4 in *Cps1*, introducing a nonsense mutation that leads to gradual decline and death with hyperammonemia and hyperglutaminemia over the course of 3 weeks[64]. The conditional knock out provides a model of human late-onset CPS1 deficiency. With controlled loss of protein and a longer time window for therapy, we demonstrated that murine Cps1 deficiency is treatable using a recombinant helper-dependent adenovirus expressing murine Cps1[64], further showing that this mouse model provides a relevant platform for developing therapies.

The goal of this work was to design and implement cell- and gene-based therapeutics for CPS1 deficiency, with both approaches applicable to all patients regardless of individual mutations. We first established CPS1 patient-derived iPSCs and edited them using CRISPR/Cas9 to introduce ectopic CPS1 expression in differentiated hepatocyte-like cells. In parallel, we used our mouse model of conditional CPS1 deficiency as a platform for developing an AAV-based treatment that does not require genome editing. The totality of this work represents the first concerted effort to establish new therapies for CPS1 deficiency in decades, and it paves the way for eventually finding a cure.

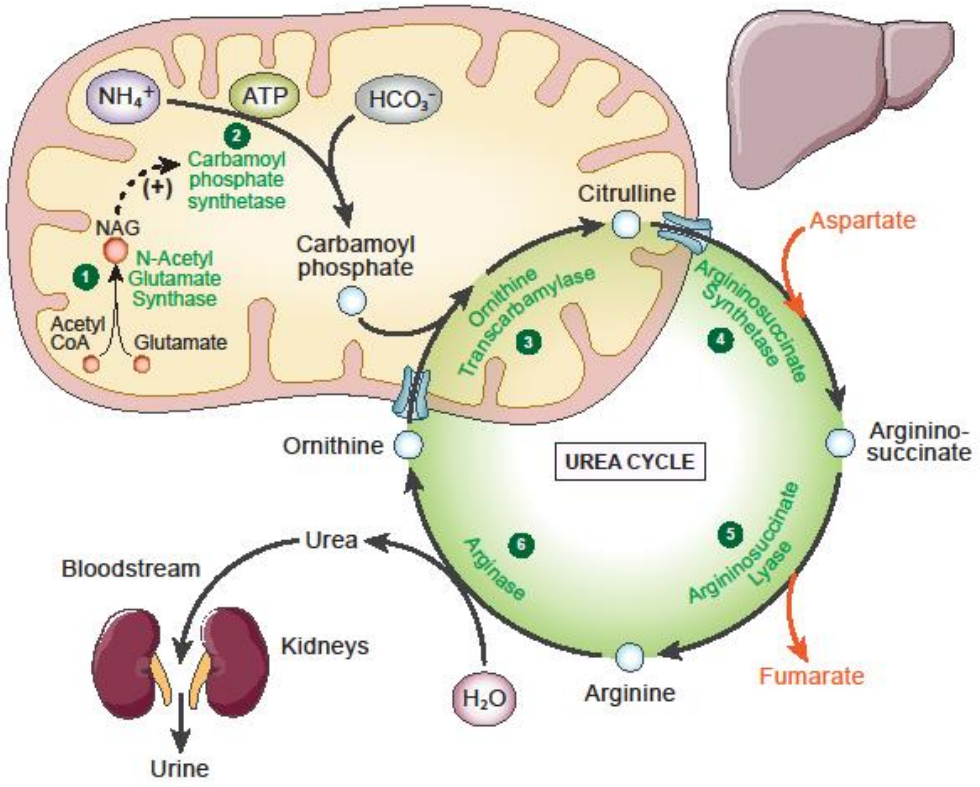

Figure 1-1. Diagram of the mammalian urea cycle. Mitochondrial CPS1 catalyzes the first step of the urea cycle by condensing ammonia with bicarbonate, generating carbamoyl phosphate that is eventually incorporated into urea and excreted by the kidneys.

Chapter 2: CRISPR-Mediated Genomic Addition to CPS1 Deficient iPSCs Is Insufficient to Restore Nitrogen Homeostasis

Introduction

Carbamoyl phosphate synthetase 1 (CPS1, EC 6.3.4.16) deficiency (OMIM #237300) is a rare inborn error of metabolism affecting the first, rate-limiting enzyme of the urea cycle, the hepatocyte function in terrestrial mammals that incorporates waste ammonia into urea for excretion; this disorder affects between 1 in 300,00 and 1 in 1.3 million worldwide[1,2]. Functional impairment or loss of CPS1 typically results in elevated plasma ammonia, leading to nausea, lethargy, encephalopathy, and coma[7]. These symptoms rapidly progress and may lead to death, even with rapid diagnosis and aggressive treatments including hemodialysis and ammonia scavenger drugs[9,10,13]. However, even if these treatments are successful in mitigating acute plasma ammonia elevations, they are incapable of preventing recurrent crises and the irreversible neurocognitive damage associated with them.

As a monogenic disorder with well-defined biochemistry, CPS1 deficiency represents a seemingly prime target for classic gene therapy approaches. Recent gene therapy successes for all the other urea cycle enzymes[51,52,65,66] also encourage this approach, but CPS1 has multiple unique hurdles that make implementing gene therapy strategies difficult, including relatively high therapeutic threshold[60] and relatively large cDNA size. These challenges were recently overcome using an adenovirus-based[64] gene replacement approach, demonstrating that lost murine Cps1 expression could be replaced with ectopic expression of murine Cps1. Though successful, the adenoviral approach is limited by potential immune complication and may be further impacted by waning efficacy over time due to episomal loss. Loss of expression may be overcome using lentivirus, but the risks from insertional mutagenesis, in addition to technical challenges in producing high titer viral preparations[67], make this approach impractical.

Cell-based therapies for metabolic disorders in general, and CPS1 deficiency in particular, may provide a viable alternative to virus-based gene therapies. Liver transplantation is generally curative but requires long-term immune suppression and faces continued scarcity in supply of donor organs[7], and rarely still requires dietary supplementation of citrulline (a key urea cycle intermediate)[20]. Patient-derived induced pluripotent stem cells (iPSCs) could circumvent the issues associated with finding compatible donor organs as well as viral delivery of genetic materials. Successful cell replacement with exogenous hepatocytes has been reported in some studies for metabolic disorders[68–70], including CPS1 deficiency[23], though rigorous and well-controlled trials remain to be performed. Human hepatocyte transplantation in an immunosuppressed murine model has previously been shown to treat another urea cycle disorder, Arginase 1 deficiency[71], effectively, and iPSC-derived hepatocytes are beginning to show similar promise in some enzyme activities when compared to primary hepatocytes[72]. One advantage of iPSC-derived hepatocyte-like cells (HLCs) is that cell quality can be controlled prior to transplantation, potentially generating a functionally unlimited supply of hepatocytes to replace the endogenous dysfunctional cells.

The discovery and implementation of the clustered regularly interspaced short palindromic repeats (CRISPR)/Cas9 gene editing platform[36,37] has revolutionized genome editing in recent years, providing a rapid and reliable tool to make precise modifications. Multiple types of mammalian cells have been edited with CRISPR/Cas9, including human iPSCs[38]. One advantage of using patient-derived iPSCs for *in vitro* editing, as opposed to primary cells *ex vivo*, is that targeted changes can be rigorously validated by sequencing prior to transplantation; in addition, potential off-target cleavage events can be predicted and mitigated through careful design, and also

subsequently confirmed. iPSCs edited with CRISPR/Cas9 have been shown to robustly express transgenes[73], including those of urea cycle enzymes[74], making this an attractive option for CPS1.

Here, we reprogrammed patient-derived CPS1 deficiency fibroblasts to iPSCs and subsequently utilized CRISPR/Cas9 to introduce ectopic CPS1 expression from the AAVS1 safe harbor locus. The resultant cells were then differentiated to HLCs to assess their ammonia metabolizing capability.

Results

Derivation and Characterization of CPS1-Deficient iPSCs

To establish a human cell model for CPS1 deficiency, we acquired three deidentified patient fibroblast lines, termed CD1, CD2, and GM03432 (subsequently referred to as GM) (Figure 2-1A). Clinical reports from all three patients indicated each had neonatal onset of disease symptoms. CD1 cells are from an afflicted male, while CD2 and GM cells are from afflicted females. CD1 cells contain a homozygous nonsense mutation resulting from the transversion c.2494G>T, leading to amino acid residue 832 converting from glutamate to a stop codon (E832X). CD2 is compound heterozygous with c.2740G>C, changing aspartate 914 to histidine (D914H), and a splice mutation resulting in exon 36 skipping (c.4162-2A>G). GM also contains a homozygous mutation, but it is missense c.610G>T, resulting in a valine to phenylalanine transition at residue 204 (V204F).

These three lines were reprogrammed using the 4 classic Yamanaka factors OCT4, SOX2, KLF4, and MYC, and clones from each cell line were used for characterization. All iPSCs exhibited typical morphology (Figure 2-1B), and gene expression analysis demonstrated that they express the pluripotency genes *OCT4*, *SOX2*, *NANOG*, *REX1*, and *TERT* at similar levels to the established human embryonic stem cell line H9 (Figure 2-1C). Immunocytochemistry showed that these cells express the pluripotency markers OCT4, KLF4, TRA-160, and TRA-181 at the protein level (Figure 2-1D). When injected into immunocompromised mice, these cells were also capable of forming teratomas with tissue derived from all three germ layers (Figure 2-1E). Karyotype analysis demonstrated that CD2 and GM iPSCs have no detectable large chromosomal aberrations (Figure 2-1F); however, CD1 was found to have a balanced translocation between the short arm of chromosome 19 and the long arm of chromosome 20. This mutation was also identified in the

parental fibroblasts, however, and was therefore not a result of reprogramming. A single clone from each line was chosen for all downstream experiments.

CRISPR/Cas9-Mediated Genomic Addition of hcoCPS1 into the AAVS1 Safe Harbor Locus

To restore CPS1 expression in deficient cell lines, human codon optimized CPS1 cDNA (hcoCPS1) was introduced into the *AAVS1* safe harbor locus using two guide RNAs with Cas9 nickase in the previously described AFP reporter cell (ARC) vector[75] with modifications. Here, the human *EF1α* promoter drives the expression of hcoCPS1, which is terminated by the human growth hormone polyadenylation sequence. An in-frame puromycin resistance gene allows for drug selection after integration, and the entire cassette is flanked by homology arms to *AAVS1*. A schematic of the genome editing strategy is depicted in Figure 2-2A.

After integration, puromycin-resistant cells were subcloned, and genomic DNA was extracted to determine if integration had been faithfully completed. PCR analysis of both the 5' and 3' junctions was performed using primer pairs amplifying from outside of the homology arms and inside the transgenic cassette (Figure 2-2A, black arrows); the expected bands were present in edited cells but not in unedited cells (Figure 2-2B). Junction PCR products were subsequently sequenced and demonstrated seamless integration of the expected genomic region and transgene sequences without errors (Figure 2-2C).

Hepatic Differentiation and In Vitro Ammonia Challenge of Edited iPSCs

To determine the capacity of these iPSCs to form hepatocyte-like cells (HLCs), iPSCs were differentiated using a previously described method[26]. Figure 2-3A depicts the overall differentiation strategy. After a 4-day endoderm induction, cells were incubated for 8 days with

hepatocyte growth factor (HGF) and dimethylsulfoxide (DMSO) to induce hepatic specification, followed by 6 days in dexamethasone, an extension of 3 days from the original protocol that modestly improves urea cycle gene expression[75]. The subsequently produced HLCs were maintained for 3 days in the presence of dexamethasone, hydrocortisone, insulin, and DMSO before being harvested for analysis on day 21. Day 21 HLCs from all three lines, both unedited and edited, exhibited the characteristic hepatocyte cobblestone morphology (Figure 2-3B), and edited cells did not statistically significantly differ from unedited cells in maturity based on expression of the immature hepatocyte gene α-fetoprotein (AFP) and mature genes cytochrome p450 3A4 (CYP3A4) and fumarylacetoacetate hydrolase (FAH) (Figure 2-3C).

To measure the ammonia consumption capacity of differentiated HLCs, NH_4Cl was added to cell media at a final concentration of 2.5mM; supernatants were harvested after 24 hours and assayed to measure ammonia levels. Unexpectedly, unedited cell supernatants contained significantly less ammonia (539.1μM ± 32) than their edited counterparts (1152μM ± 62; $p < 0.0001$) (n = 3 for each cell line, total of n = 9 per group) (Figure 2-3D).

Investigating Potential Mechanisms of Differential Ammonia Metabolism

To address the unexpected results from the *in vitro* ammonia challenge, RNA was extracted from HLCs and subjected to qPCR analysis for the 6 enzymes and 2 transporters of the urea cycle, in addition to hcoCPS1, to further assess function (Figure 2-4A). There were no significant differences in gene expression between unedited and edited HLCs (n = 3 per cell line, total n = 9 per group) except for endogenous *CPS1* (0.52-fold ± 0.15 relative to unedited cells; $p = 0.017$). Unexpectedly, hcoCPS1 expression was not markedly elevated in edited cells (1.82-fold ± 0.4 relative to unedited cells; $p = 0.22$), prompting investigation into its poor expression. Loss of

hcoCPS1 expression was not due to heterochromatin formation as these cells retained puromycin resistance (data not shown), suggesting some other mechanism was responsible. DNA methylation is one method of gene regulation in which cytosine residues in CpG dinucleotides are covalently methylated at the fifth position of the pyrimidine ring to form 5-methylcytosine; this event is commonly associated with transcriptional silencing[76], and global DNA methylation status is known to fluctuate during differentiation[77]. To determine the DNA methylation status at the transgene promoter in HLCs, genomic DNA was extracted and subjected to bisulfite conversion. Bisulfite conversion deaminates cytosine into uracil but has no effect on 5-methylcytosine. Subsequent sequencing can demonstrate if cytosines were protected from conversion by a methyl group, providing insight into local DNA methylation states. All three edited lines demonstrated methylation at all 19 CpG dinucleotides in the transgenic *EF1α* promoter, in addition to 7 CpGs in the flanking DNA (2 of them upstream and the remaining 5 downstream of the promoter) (Figure 2-4B). Unexpectedly, promoter methylation was not a result of differentiation as undifferentiated iPSCs also showed complete methylation (Figure 2-4C). The donor plasmid used during nucleofection showed no methylation (Figure 2-4C), indicating that promoter methylation was iPSC-derived after integration. Loss of hcoCPS1 expression was confirmed in iPSCs; shortly after CRISPR/Cas9 editing and puromycin selection, edited iPSCs showed significantly increased expression of hcoCPS1 (26.02-fold ± 11.16 compared to unedited; $p = 0.040$) (Figure 2-4D) which was lost upon subsequent culturing (1.76-fold ± 0.68 compared to unedited; $p = 0.7$) (Figure 2-4E). Transcriptional silencing was accompanied by undetectable levels of CPS1 enzyme activity in edited iPSCs (data not shown).

While promoter methylation explains the loss of hcoCPS1 expression, it fails to account for the difference in ammonia reduction between unedited and edited HLCs. Hepatocytes *in vivo*

are central in regulating amino acid metabolism[78], including those whose synthesis involves the incorporation of ammonia. The reversible production of glutamine involves the condensation of glutamate with ammonia, regulated by glutamine synthetase (GLUL) and glutaminase 2 (GLS2). In addition, glutamate itself is reversibly produced from ammonia and α-ketoglutarate via the action of glutamate dehydrogenase (GLUD1). Because hcoCPS1 expression is lost in edited cells, we hypothesized that differential expression of any of these three metabolism genes could account for varying levels of ammonia utilization in HLCs. qPCR analysis showed that none of these three genes were significantly differentially expressed between unedited and edited HLCs (*GLUL*: 1.65 ± 0.33, p = 0.1; *GLS2*: 2.52 ± 1.05, p = 0.2; *GLUD1*: 1.19 ± 0.37, p = 0.6 [all compared to unedited cells])(Figure 2-4F).

Discussion

CPS1 deficiency is an inborn error of metabolism in which ureagenesis stalls due to lack of input carbamoyl phosphate from the CPS1 protein. Symptoms typically arise in the neonatal period, though onset may occur at any time in childhood or into adulthood depending on the extent of protein dysfunction, with as many as 50% of neonatal cases leading to mortality[2]. Dietary protein restriction and ammonia scavenger drug administration are the mainstays of current therapy, but they are incompletely effective and have remained largely unchanged since the 1980s; orthotopic liver transplantation is generally curative, though donor organs remain scarce and are accompanied by lifelong immune suppression and in some cases patients still require additional citrulline supplementation[20]. Currently, there are no treatments that fully address the underlying biochemical imbalance or reverse the accumulated neurocognitive deficits from repeated episodes of hyperammonemia.

To develop a novel therapeutic option for CPS1 deficiency patients, we reprogrammed patient-derived fibroblasts into iPSCs and inserted human codon optimized CPS1 cDNA into the *AAVS1* locus for constitutive expression via the *EF1α* promoter using CRISPR/Cas9. Edited iPSCs were differentiated to hepatocyte-like cells (HLCs) to determine their ammonia metabolizing capacity relative to their isogenic, unedited controls. Upon challenging with NH_4Cl, edited HLCs removed significantly less ammonia from the supernatant than unedited HLCs. This result was unexpected as overexpression of hcoCPS1, in the presence of similar expression levels of the other urea cycle enzymes, would be expected to increase ammonia utilization. However, upon further investigation, hcoCPS1 was found to be silenced due to promoter methylation. *AAVS1*-based transgene insertion and expression is a long-standing concept in stem cell biology, with many reported successes[79,80]. However, transgene silencing at *AAVS1* mediated by promoter methylation

has also been reported in undifferentiated[81] and differentiated[79] cells. These and previous studies suggest that promoter choice is a critical component in avoiding silencing; previous work from us and others[74,82] has demonstrated that the *EF1α* promoter expresses well in PSCs, suggesting some other factor that remains to be elucidated is impacting methylation status. Cell-line specific alterations may also exist, and potentially global DNA methylation changes, that could explain the difference in unedited and edited cells. Determining the causal factors of promoter silencing will be important in moving transgenic PSC technologies towards more translatable therapies.

The difference in ammonia utilization in unedited and edited HLCs, despite no obvious urea cycle-related gene expression differences, suggests that unedited HLCs shuttled ammonia into an alternative pathway. In addition to urea, ammonia may be condensed with α-ketoglutarate to form glutamate by the enzyme glutamate dehydrogenase (GLUD1, EC 1.4.1.3). Glutamate may then receive an additional ammonia moiety to form glutamine via glutamine synthetase (GLUL, EC 6.3.1.2). Both reactions are reversible either by GLUD1 itself or by the action of glutaminase 2 (GLS2, EC 3.5.1.2), respectively. Together, these three enzymes represent a small portion of urea cycle-independent enzymes that directly affect ammonia levels in hepatocytes, making them attractive targets to investigate as potential differential regulators of ammonia levels in unedited and edited HLCs. However, their gene expression levels were not significantly different between the two cell populations, suggesting that if they are playing a role, it is post-transcriptional. Metabolic flux through these enzymes may be investigated using metabolomics approaches with isotopic nitrogen-containing compounds, as has been done previously in other disease contexts[83], which may also clarify the roles of alternate processes affecting ammonia indirectly, such as amino acid uptake, in an unbiased way.

While there is great potential for iPSC-derived HLCs as a therapeutic, they do have important disadvantages. One significant drawback is the time needed to generate, edit, and differentiate the cells to the desired fate. However, CPS1 deficiency can be diagnosed prenatally by amniocentesis[84], taking advantage of a key time window during which the unborn fetus relies on maternal ammonia clearance. This approach would potentiate the development of a cell-based therapeutic tailored to the patient that is ready for administration at or soon after birth. Recent advances in liver organoids[85] and scaffolding for transplantation[43] bring the potential of near-to-medium-future hepatocyte replacement therapies into sharper focus. As CPS1 deficiency has been treated in limited cases with primary hepatocyte transplantation[23], this approach has untapped therapeutic potential, especially in the context of ongoing donor liver scarcities[86].

In conclusion, we have demonstrated that CPS1 patient-derived iPSCs successfully generate hepatocyte-like cells, but that *EF1α* promoter-driven hcoCPS1 expression from the *AAVS1* safe harbor is not suitable to reconstitute the urea cycle. This work lays a foundation for future studies investigating alternative promoter constructs and *cis*-regulatory elements to optimize transgene expression in differentiated cells and restore expression of this critical hepatic protein.

Materials and Methods

Cell Lines and Reprogramming

Deidentified CPS1 deficiency patient fibroblasts were purchased from Coriell Institute for Medical Research (GM03432) or were a generous gift from Johannes Häberle (CD1 and CD2). The mutation in GM03432 cells was identified by exome sequencing performed by Prevention Genetics (Marshfield, WI). Fibroblasts were cultured on 0.1% gelatin (StemCell Technologies, 07903) in DMEM/F12 (11320033) supplemented with 20% fetal bovine serum (FBS; 10437028), 1% glutaMAX (35050061), 1% non-essential amino acids (NEAA; 11140050, all from Invitrogen), and primocin (Invivogen, ant-pm-1). Fibroblasts were reprogrammed using the lentiviral STEMCCA vector expressing the 4 Yamanaka factors as described previously[74] and were subsequently cultured on irradiated mouse embryonic fibroblasts (ThermoFisher, A34180) in mTeSR Plus growth media (StemCell Technologies, 100-0276) until colonies emerged. Clones were picked and transduced with AAV8-Cre (a gift from James M. Wilson, Addgene viral prep 105537-AAV8) to remove the STEMCCA cassette. Genomic DNA was harvested (Qiagen, 69504), and STEMCCA removal was confirmed by PCR as described previously (Center for Regenerative Medicine [CReM] iPSC Core of Boston University and Boston Medical Center https://www.bu.edu/dbin/stemcells/index_iPSC.php). Primers for STEMCCA PCR were: Forward: 5'- TGGCTCTCCTCAAGCGTATT-3'; Reverse: 5'-GTTGTGCATCTTGGGGTTCT-3'. iPSCs were routinely maintained on hESC-qualified Matrigel (Corning, 354277) in mTeSR Plus and passaged using ReLeSR (StemCell Technologies, 05872) according to the manufacturer's instructions.

Immunocytochemistry

iPSCs were probed for pluripotency markers as described previously[74]. Primary antibodies used were: OCT3/4 (Santa Cruz Biotechnology, SC-5279); KLF4 (Stemgent, RC-09-0021); TRA1-60 (Millipore, mab4360); TRA1-81 (Millipore, mab4381) all at 1:200 dilutions. Secondary antibody used was goat anti-mouse IgG Alexa Fluor 488 (Life Technologies, A-11001) at 1:200 dilution.

qPCR

qPCR was performed as previously described[87]. Briefly, total RNA was isolated, and cDNA synthesized according to manufacturer's instructions (Roche, 11828665001 and 4897030001, respectively). qPCR was carried out using BioRad ssoAdvanced Universal SYBRGreen (Hercules, CA, 1725271). A list of primers used can be found in Table 2-1. *GAPDH* was used as the housekeeping gene, and fold changes were calculated using the -ΔΔCt method.

Teratoma Assay

All mice were kept according to the National Institutes of Health guidelines and all experimental procedures were approved by and conducted according to the guidelines of the Institutional Animal Care and Use Committee of the University of California, Los Angeles. Mice had *ad lib* access to standard chow and water and were maintained on a 12-hour light-dark cycle. Severe combined immunodeficient mice (NGS, Jackson Laboratory) were anaesthetized with isoflurane, and 10 million iPSCs suspended in Matrigel were injected unilaterally into the quadriceps. Mice were euthanized when visible tumors formed, and the tissue was fixed in 10% buffered formalin for 48 hours. Teratomas were embedded in paraffin, sectioned, and stained with hematoxylin and eosin for imaging.

Hepatic Differentiation

iPSCs were differentiated to hepatocytes as described previously[26] with modifications. Undifferentiated iPSCs were incubated in 10µM Y-27632 ROCK inhibitor (BioPioneer, SM-008) for 1 hour and subsequently dissociated using Accutase (ThermoFisher, A1110501). Cells were then seeded onto Matrigel (Corning, CB-40230C) at a density of 2 million per well of a 6-well plate (approximately $2.1x10^5$ cells/cm^2). The following day, cells were induced to form endoderm using the STEMDiff Definitive Endoderm kit (StemCell Technologies, 5110) for 4 days. Endodermal cells were then replated at ~50% density (empirically optimized for each individual cell line) in differentiation media made with DMEM/F12 containing 10% knockout serum replacement (Invitrogen, 10828028), 1% NEAA, 1% glutaMAX, and primocin. This was further supplemented with 1% DMSO (Sigma Aldrich, D8418-500ML) and 100ng/mL hepatocyte growth factor (StemCell Technologies, 78019) for 8 days. Cells were then cultured for 6 days in differentiation media supplemented with 0.1µM dexamethasone (Sigma-Aldrich, D4902-25MG). Finally, cells were matured for 3 days in William's E media (Invitrogen, 12551032) containing 10% FBS, 1% NEAA, 1% glutaMAX, 1.8% DMSO, 1µg/mL human insulin (Sigma-Aldrich, I9278-5ML), 4.8µg/mL hydrocortisone 21-hemisuccinate (Sigma-Aldrich, H2270-100MG), and 0.1µM dexamethasone. Media was changed daily throughout the differentiation. Cells were harvested using 0.25% trypsin (Invitrogen, 25200056).

Molecular Cloning and CRISPR/Cas9 Genome Editing

Human codon-optimized *CPS1* (hcoCPS1) was synthesized by Blue Heron Biotech (Bothell, WA) as previously described[87]. hcoCPS1 was cloned into the ARC vector and inserted

into the *AAVS1* site as described previously[75]. Briefly, NEBuilder HiFI DNA Assembly (New England Biolabs, E2621S) was used to introduce *EF1α*-driven hcoCPS1 into ARC, which was subsequently confirmed by sequencing, replacing the original transgenic construct and forming the new donor. This donor was nucleofected into iPSCs along with paired Cas9 nickases (a gift from Feng Zhang[39], Addgene #48140) targeting *AAVS1*, using the Amaxa Nucleofector program B016. Treated cells were then selected with puromycin at 1ug/mL. Clones were isolated and screened by PCR using the primers in Table 2-1. Faithful transgene integration was confirmed by sequencing (Laragen).

In Vitro Ammonia Challenge

Day 20 HLCs were treated with 2.5mM $^{15}NH_4Cl$ (Cambridge Isotope Laboratories, NLM-467-1), and supernatant was harvested after 24h and stored at -80°C until analysis. Ammonia levels were detected using a colorimetric ammonia assay (Abcam, ab83360) according to the manufacturer's instructions.

DNA Methylation Analysis

Genomic DNA from iPSCs and HLCs was isolated (Qiagen, 69506) and subsequently bisulfite converted (Zymo Research, D5005) according to the manufacturer's instructions. The bisulfite-converted 231bp core *EF1α* promoter was PCR amplified and sequenced. Primers were designed using the Zymo Bisulfite Primer Seeker tool and are listed in Table 2-1.

Statistical Analysis

Collected data was analyzed with the Prism8 (GraphPad Software) statistical package. Results were expressed as mean ± standard error of the mean (SEM) and p values were determined using one-way ANOVA with Tukey's multiple comparison's test, or unpaired T-test when applicable. $p < 0.05$ was considered significant.

A

Line Name	Sex	Disease Onset	Mutation
CD1	Male	Neonatal	E832X
CD2	Female	Neonatal	D914H c.4162-2A>G
GM	Female	Neonatal	V204F

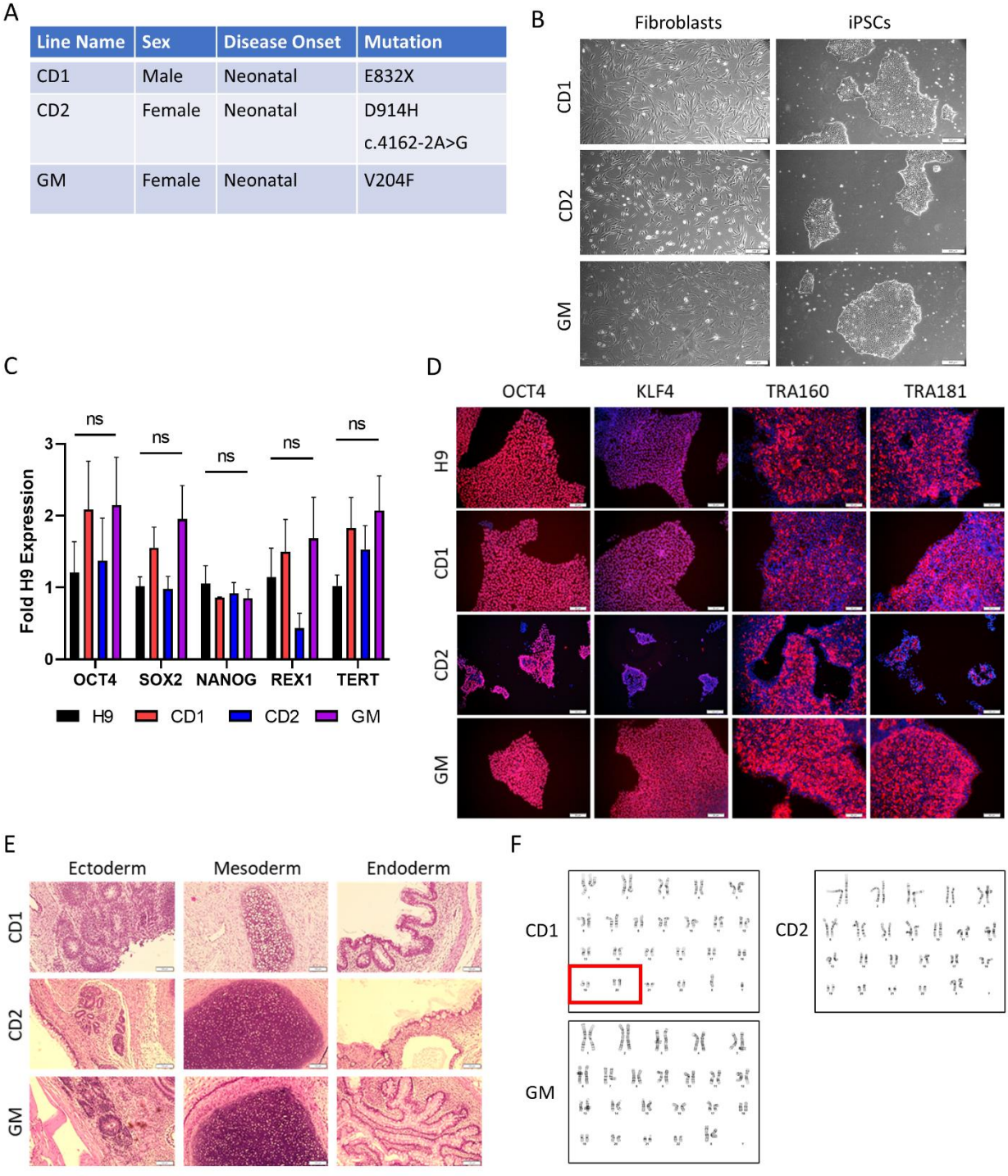

Figure 2-1. Characterization of patient-derived iPSCs. **A**) Table detailing the mutations in the three cell lines. CD1 and GM are both homozygous, while CD2 is compound heterozygous. **B**) Bright field images of patient-derived parental fibroblasts and their corresponding daughter iPSCs. **C**) qPCR analysis of pluripotency genes in patient iPSCs compared to the human embryonic stem cell line H9. Data are mean ± SEM, n = 3 per group. **D**) Immunocytochemistry of pluripotency markers in iPSCs compared to H9 cells. **E**) H&E staining of sections from teratomas formed by

each cell line. All three lines generate tissues derived from the three primary germ layers. **F**) Karyotype analysis of CD1, CD2, and GM iPSCs. Red box in CD1 indicates balanced chromosomal translocation between chromosomes 19 and 20.

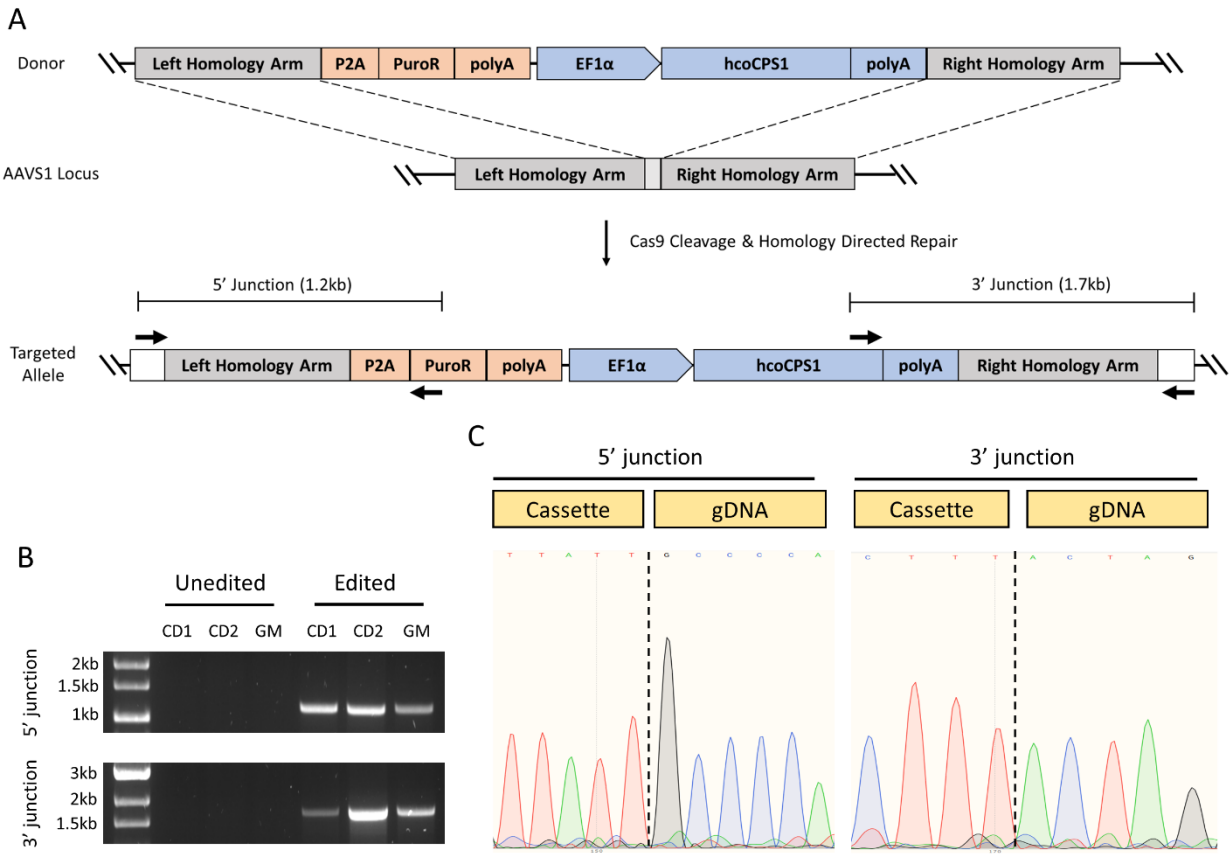

Figure 2-2. Design and validation of CRISPR/Cas9 editing in iPSCs at the *AAVS1* locus. **A**) Schematic of the overall CRISPR/Cas9 strategy. **B**) Gel images of PCRs amplifying either the 5' or 3' junctions, defined by the bracketed lines in A. Primer locations are indicated by black arrows in A. **C**) Sequencing of the 5' and 3' junctions showing faithful insertion of the transgenic construct.

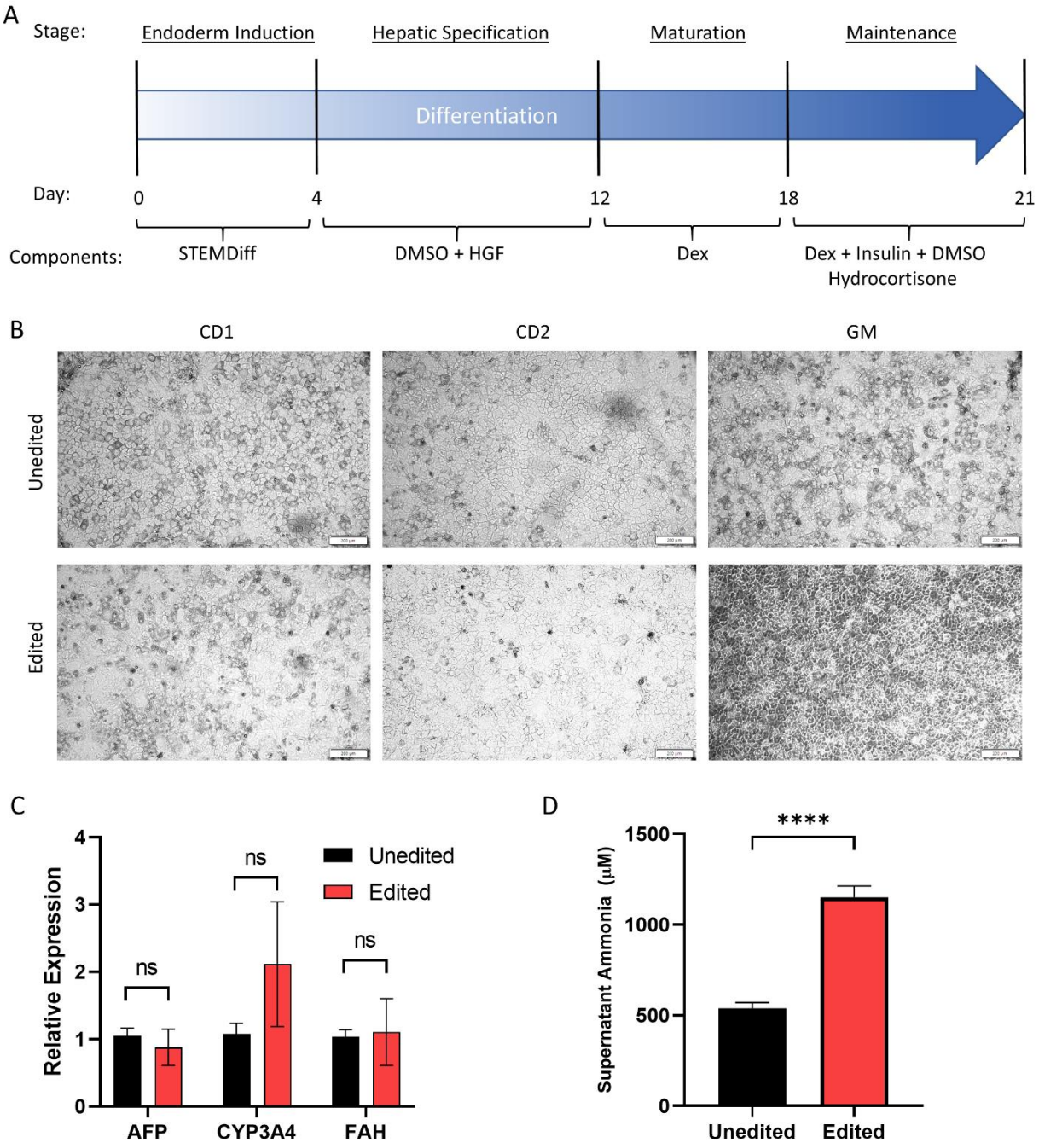

Figure 2-3. Differentiation of iPSCs to HLCs. **A**) Schematic diagram of the hepatic differentiation strategy. iPSCs are directed progressively through the definitive endoderm, hepatic specification, and maturation stages, using the listed growth factors to reach the HLC state. **B**) Representative bright field images of day 21 HLCs from all three lines with and without CRISPR/Cas9 genome editing. No salient morphological differences were observed. **C**) qPCR analysis of unedited and edited day 21 HLCs. Expression of the less mature *AFP* and more mature *CYP3A4* and *FAH* genes are not significantly different between the two. **D**) Levels of ammonia found in the supernatant of day 21 HLCs after 24 hours of treatment with 2.5mM NH_4Cl. ****$p < 0.0001$. Data in C and D are mean ± SEM, n = 9 per group.

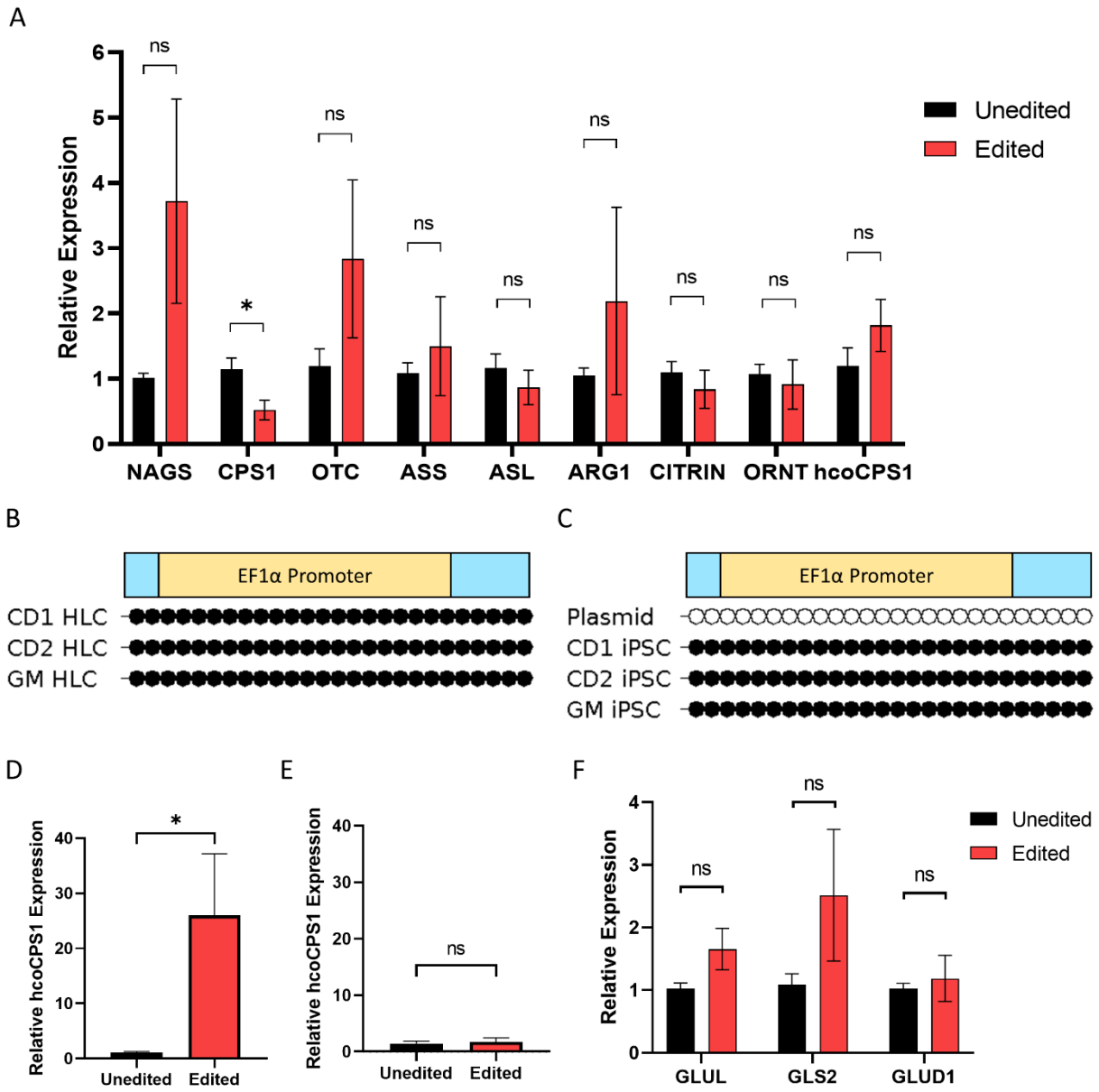

Figure 2-4. Investigating the factors contributing to differential ammonia metabolism in unedited and edited HLCs. **A**) qPCR of urea cycle-related genes (6 enzymes and 2 transporters) in day 21 HLCs. **B and C**) DNA methylation analysis of edited day 21 HLCs (B) and edited iPSCs with donor plasmid control (C). All CpGs showed methylation, including those up- and downstream of the promoter (blue rectangles). **D and E**) qPCR analysis of hcoCPS1 in unedited compared to edited iPSCs after only a few passages (D) and several passages (E). **F**) qPCR analysis of glutamate/glutamine metabolic genes in day 21 HLCs. Data in D-F are mean ± SEM, n = 9 per group. *p < 0.05.

Table 2-1. Primers list

Primer Name	**Sequence (5'-3')**
qPCR	
GAPDH F	GCTCTCTGCTCCTCCTGTTC
GAPDH R	ACGACCAAATCCGTTGACTC
NAGS F	CAGTTCCAGACCTGCCATCACT
NAGS R	ATGTCCATGCGCTGCAAGAAGG
Endogenous CPS1 F	CAAGTTTTGCAGTGGAATCG
Endogenous CPS1 R	ACGGATCATCACTGGGTAGC
hcoCPS1 F	TACCCAACAACCTTGCTGTACCTC
hcoCPS1 R	GAGCTTGAGCGACTTTGAGTTCGT
OTC F	CCAGAGGCAGAAAACAGAAAG
OTC R	TTCTTGACAAGTAACACAACATCAAA
ASS1 F	CTTGGAGCTCTTCATGTACC
ASS1 R	GATACCTCGGGACTTCATTC
ASL F	TCGCTGTGCATGACCCATC
ASL R	CCAAACTGTCGGGGTTTTTCT
Arg1 F	TGGACAGACTAGGAATTGGCA
Arg1 R	CCAGTCCGTCAACATCAAAACT
CITRIN F	CACCAGGAAAGATGTTGAAGTG
CITRIN R	TCCATGGGTGTAACCTGACC
ORNT F	TTGCATCAGGGAGATCAAAA
ORNT R	GCAAGCCAGAGGCAAATC
AFP F	TGTACTGCAGAGATAAGTTTAGCTGAC
AFP R	TCCTTGTAAGTGGCTTCTTGAAC
CYP3A4 F	AAGTCGCCTCGAAGATACACA
CYP3A4 R	AAGGAGAGAACACTGCTCGTG
FAH F	ACCAGGATGTCTTCAATCAGC
FAH R	CAAGAACACTCTCGCCTCCT
GLUD1 F	CCATGGAGCTAGCAAAAAAGGG
GLUD1 R	TGATGGGTTTACCAGTAACACAG
GLS2 F1	CCAGCCAAGTCAGCTGTAT
GLS2 R1	AGACACCAACTTCTGGCAG
GLUL F	ATACGCTTGACTTTCTGTGGCTG
GLUL R	ATGGCCTGGACTTTCTCACC
Junction PCRs	
5' Junction F	GCTCAGGTCTGGTCTATCTGCCTGG
5' Junction R	CACCGTGGGCTTGTACTCGGTCA
3' Junction F	GCCGTGGATAGCGGTATCCC
3' Junction R	CCGAAGAGTGAGTTTGCCCAAGC

DNA Methylation	
EF1α Promoter F	TAAGGGGGAGGATTGGGAAG
EF1α Promoter R	AAAAATCACRTACTACAACCAAATA

Chapter 3: Split AAV-Mediated Gene Therapy Restores Ureagenesis in a Murine Model of Carbamoyl Phosphate Synthetase 1 Deficiency

Introduction

Carbamoyl phosphate synthetase 1 (CPS1; E.C. 6.3.4.16) catalyzes the ATP-dependent condensation of ammonia and bicarbonate into carbamoyl phosphate[88], which subsequently proceeds through the urea cycle in hepatocytes or the arginine biosynthesis pathway in intestinal epithelium[89]. CPS1 resides in the mitochondria, where its function is dependent on the allosteric activator n-acetylglutamate (NAG). CPS1 deficiency (OMIM #237300) is a rare autosomal recessive disorder caused by mutations in the *CPS1* gene leading to diminished or abolished CPS1 protein function. The estimated incidence is 1 in 1.3 million in the United States and Europe[1], though estimates vary widely[2], which is likely an underestimate due to the difficulty in making an accurate early diagnosis.

Patients afflicted with CPS1 deficiency often present in the neonatal period with vomiting, lethargy, and coma due to elevated plasma ammonia. With acute life-threatening episodes of hyperammonemia, hemodialysis may be necessary. Timely and aggressive treatment is essential for reducing plasma ammonia to prevent mortality; however, these treatments are typically unable to prevent marked hyperammonemic episodes and cannot reverse neurological injury that has been acquired during these crises. Even in the best of circumstances, patients often remain severely nitrogen vulnerable. Current chronic treatment strategies rely primarily on dietary protein restriction and ammonia scavenger administration in combination with L-arginine and/or L-citrulline supplementation[90].

Recent advances in gene therapy have led to the concept of treating CPS1 deficiency using adeno-associated virus (AAV)-based technology; as a monogenic disorder that is a well-defined enzyme deficiency with no completely effective medical treatment except liver transplantation (which has accompanying inherent risks, both short- and long-term), it is an appropriate disorder

to target for therapeutic advances. While AAV-mediated gene transfer has proven effective in animal models for other urea cycle disorders including deficiencies of ornithine transcarbamylase[52], argininosuccinate synthetase[66], argininosuccinate lyase[65], and arginase 1[51], no gene therapy strategies using AAV have yet been established for CPS1 deficiency for multiple reasons. First, until recently there were no viable animal models of CPS1 deficiency. While a neonatal murine model was developed 20 years ago[62], this was not submitted to a repository and was lost for future investigation[63]. In that model, neonatal mice perished within the first 24 hours after birth; developing therapies in a newborn mouse with the early intake of milk and consequent early rise in plasma ammonia poses significant challenges. As an alternative to the neonatal model, an adult model of CPS1 deficiency was recently established utilizing primary human hepatocytes from patients transplanted into immune compromised mice and expanded *in vivo*[91]. However, this model suffers from being technically challenging and time consuming, in addition to requiring access to a relatively rare cell population. Second, CPS1, being the most abundant mitochondrial protein in human liver, must be expressed at high levels in hepatocytes. The enzyme itself accounts for 15-20% of the total mitochondrial protein as a 165,000 molecular weight polypeptide[88]; its expression is pan-hepatic[92,93], not exclusively periportal like some of the other urea cycle enzymes, further leading to challenges of obtaining adequate expression. This is in contrast to gene therapy targets such as hemophilia that require as little as 1-2% protein levels to achieve therapeutic benefit[94]. Finally, the size of the CPS1 cDNA at 4.5kb, and limitations of the transgene expression cassette to 4.7kb to maximize packaging efficiency, may be the greatest hindrance for a clinically translatable vector that can be produced at high titer such as AAV; with inverted terminal repeats and regulatory elements, the genome size easily exceeds the canonical limit of AAV.

Vector systems exist to package and deliver large transgenes, though they have significant drawbacks. Adenoviral vectors are highly immunogenic[45], while lentiviral vectors suffer from low titer and random, widespread genomic integration[95]. Plasmids can be difficult to deliver and are largely silenced due to the presence of bacterial genomic elements[96]. To overcome these limitations, an approach was developed to capitalize on the recombinogenic nature of AAV vectors. This is achieved by generating two separate AAVs that contain complementary halves of a transgene cassette that includes a region of homology between them. These so-called dual or split AAVs (sAAVs) can potentiate homologous recombination between the vectors upon co-transduction of the same cell[97,98], resulting in expression of the full-length therapeutic transgene. Variations on this system include relying on ITR-mediated concatemerization and subsequent removal by splicing, known as *trans*-splicing[97], and the hybrid[99] approach, which combines elements from both the overlapping and *trans*-splicing approaches. sAAV approaches have been implemented successfully in, amongst others, the retina for Alström syndrome[100], skeletal muscle for dysferlin deficiency[101], and the liver for glycogen storage deficiency type III[102].

Here we describe the design and implementation of a sAAV dual vector approach to treat CPS1 deficiency. Using our recently established conditional knockout murine model of CPS1 deficiency[64], we demonstrate that sAAV-mediated gene transfer is able to restore CPS1 hepatic expression, control plasma ammonia, and re-establish ureagenesis. These studies lay the proof-of-concept groundwork for a clinically translatable gene therapy approach to treat CPS1 deficiency.

Results

In Vitro Transduction with sAAVs Leads to RNA and Protein Expression of hcoCPS1

A schematic of the sAAV strategy is depicted in Figure 3-1A. Two separate viral vectors were prepared: the first (5' [or left] sAAV) contains the constitutively active CMV enhancer/chicken β-actin promoter (CAG) and the 5' half of the human codon-optimized *CPS1* transgene (hcoCPS1) (cDNA base pairs 1-2181); the second virus (3' sAAV [or right]) contains the 3' half of hcoCPS1 (cDNA base pairs 1714-4521) and the rabbit β-globin polyadenylation sequence. A 467bp region of homology within the transgene (overlap) potentiates homologous recombination upon co-transduction of the same cell, resulting in the reconstituted full-length transgene with no intervening viral ITR (combined sAAV).

To determine if sAAVs containing hcoCPS1 have the same propensity for homology-directed concatemerization as previously tested transgenes by others[98,103], HEK 293T cells were transduced with sAAVs followed by genomic DNA extraction. There was a dose-dependent increase (log increments from 10^2 to 10^5 viral genomes/cell) in detectable concatemerized product when amplified using primers to specifically recognize either the 5' (primers LF and LR), 3' (primers RF and RR), or combined sAAV (primers LF and RR) (Figure 3-1B; primers shown as black half-arrows in Figure 1A). To show that concatemerization leads to gene and protein expression, HeLa and 293T cells were transduced, and RNA and protein, respectively, extracted. Gene expression analysis by qPCR demonstrated that the individual halves of hcoCPS1 are only detectable in cells transduced with the relevant sAAV (relative to non-transduced cells) (Figure 3-1C; primers shown as red/blue arrows in Figure 3-1A). CPS1 protein levels were also increased over endogenous levels in 293T cells transduced with both sAAVs (2.7-fold increase relative to non-transduced cells) (Figure 3-1D).

In Vivo sAAV Treatment Extends Lifespan of Cps1-Deficient Mice

Following *in vitro* testing, sAAVs were tested for therapeutic efficacy *in vivo*. A diagram of the general workflow is depicted in Figure 3-2A. To determine the optimal viral dose for subsequent *in vivo* studies, adult female Cps1 conditional knockout mice (*Cps1*$^{flox/flox}$) were injected with AAV8-Cre and increasing doses of sAAVs ranging from $1x10^{13}$ genome copies (GC)/kg to $3x10^{14}$ GC/kg of each virus (Figure 3-2B; n = 3 per dose). The minimum dose required to extend lifespan to 30 days in all mice in a group was $3x10^{14}$ GC/kg. Because the mice at the highest dose still showed a slight decline in body weight (data not shown), a surrogate for overall health, in addition to our previous work demonstrating that therapeutic CPS1 level requirements are relatively high[64], all subsequent studies were carried out with $5x10^{14}$ GC/kg/virus. No acute or chronic side effects were seen at this dose, and plasma alanine aminotransferase levels (ALT, collected on day 36) were not significantly different from control mice (sAAV-treated: 31.8 ± 3.0 U/L, n = 4; wild type: 37.8 ± 12.7 U/L, n = 5; p = 0.69) (Figure 3-2C).

To investigate the ability of sAAVs to treat CPS1 deficiency, adult *Cps1*$^{flox/flox}$ mice were injected with AAV8-Cre alone (referred to as *untreated*) or in combination with sAAVs at $5x10^{14}$ GC/kg (referred to as *treated*; n = 5 each for both males and females, all groups). At this dose, both female and male mice survived beyond 120 days (Figure 3-2D), significantly longer ($p < 0.0001$) than untreated controls that perished by day 22 (females: range 19-22 days) or 21 (males: range 17-21 days).

The studies with the female mice began first. All untreated Cps1$^{-/-}$ mice (Figure 3-2E, black line) had significant weight loss and died or were euthanized due to humane endpoints by day 22. By day 38, treated female Cps1$^{-/-}$ mice began to slowly lose weight (10% of their starting weights)

(Figure 3-2E, red line). As an additional intervention in the treated $Cps1^{-/-}$ mice, n-carglumic acid (NCA), a structural analog of the Cps1 allosteric activator NAG, was added to the drinking water to increase CPS1 activity (Figure 3-2E, red arrow F1); dextrose (5%) was also included in the water to encourage consumption. Dextrose/NCA-treated female mice subsequently regained the lost weight and continued to gain over time (red line). These mice were dependent on this supplementation as its withdrawal (red arrow F2) resulted in weight loss prior to re-administration (beginning at red arrow F3). In addition, NCA treatment alone, without dextrose, was sufficient to maintain stable weights (Figure 3-2E, red arrow F4) and plasma ammonia levels (Figure 3-2F, $p = 0.8$). With these findings in the female mice, male mice (blue line) were subsequently administered water with dextrose/NCA beginning at day 14 (blue arrow M1).

sAAV Treatment Improves Biochemical Profiles of Cps1-Deficient Mice

To understand the extent of the therapeutic response, plasma ammonia was measured in untreated, sAAV-treated, and wild type mice (n = 5 per group for both males and females). At day 21, plasma ammonia levels in treated mice (red line) were significantly lower than untreated control mice (black line) in both females (339.0 ± 42.3 µM vs. 1244.6 ± 180.9 µM [treated vs. untreated, respectively], $p < 0.01$) and males (581.3 ± 60.9 µM vs. 1090.4 ± 166.7 µM, $p = 0.021$) (Figure 3-2G and H). At 120 days, compared to baseline (Day 0) levels, females (138.9 ± 38.7 µM [Day 0] vs. 464.3 ± 65.0 µM [Day 120], $p = 0.026$) and males (231.8 ± 41.9 µM [Day 0] vs. 601.0 ± 53.7 µM [Day 120], $p = 0.033$) demonstrated controlled plasma ammonia, albeit females with superior control.

To further investigate metabolic health, untreated, sAAV-treated, and wild type mice underwent urea cycle-related plasma amino acid profiling to determine the extent of residual

metabolic derangement (Figure 3-3). In untreated female mice (black line) compared to wild type controls (blue line), though not statistically significantly, arginine trended towards reduction ($p = 0.067$) (Figure 3-3A), while citrulline ($p = 0.70$) and ornithine were not significantly reduced (Figure 3-3B and C, black lines). In contrast, glutamine was significantly elevated in Cps1 deficiency at the time of death relative to wild type controls (853.4 ± 74.9μM vs. 630.6 ± 18.9μM; $p = 0.03$) (Figure 3-3D). Alanine, a non-toxic molecular carrier of nitrogen, was reduced at baseline (269 ± 9.5μM vs. 356.2 ± 8.0μM, $p < 0.01$) but increased slightly by day 21 in $Cps1^{-/-}$ mice when they perished ($p = 0.5$), while glutamate did not significantly increase (Figure 3-3F). Conversely, sAAV-treated females (red line) showed no significant differences compared to wild type mice in plasma arginine, citrulline, glutamate, and glutamine (Figure 3-3A, B, D, and F [red lines], respectively). Ornithine was significantly reduced in treated mice at days 21 (38.1 ± 5.8μM; $p = 0.03$) and 60 (36.5 ± 4.1μM; $p = 0.02$) compared to wild type controls (64.2 ± 3.9μM), though not at days 30 and 120 ($p = 0.8$ and 0.13, respectively) (Figure 3-3C). Alanine levels were not significantly elevated compared to wild type controls (Figure 3-3E).

Like the female mice, untreated $Cps1^{-/-}$ males (black line) showed a trend towards reduced arginine levels compared to wild types (50.6 ± 5.2μM vs. 64.6 ± 4.1μM; $p = 0.066$) (Figure 3-3G) while citrulline was also reduced, however not significantly different from wild type controls (Figure 3-3H). Ornithine was significantly reduced at time of death compared to wild type mice (30.6 ± 5.9μM vs. 45.2 ± 2μM, $p = 0.047$) (Figure 3-3I) while plasma glutamine was significantly elevated compared to wild type mice (932.9 ± 73.1μM vs. 487.3 ± 46μM; $p < 0.001$) (Figure 3-3J), as expected; however, alanine and glutamate showed no significant differences in untreated $Cps1^{-/-}$mice compared to wild type controls (Figure 3-3K and L). In contrast, treated male mice (red line) had significantly elevated arginine at days 21, 30, and 60 (peak at day 30: 109.7 ±

12.9μM, p = 0.01) compared to wild type mice (Figure 3-3G). Citrulline was also significantly elevated at days 60 and 120 compared to wild type mice (peak at day 60: 104.9 ± 10μM vs. 67.2 ± 8.3μM, p = 0.019) (Figure 3-3H) while ornithine was significantly reduced at days 21 and 60 (trough at day 60: 33 ± 0.9μM, p < 0.001), though not at days 30 and 120 (Figure 3-3I). Similar to untreated controls, glutamine was significantly elevated in treated mice from day 21 to the end of the study at day 120 (peak at day 60: 1090 ± 96.9μM, p < 0.001) compared to wild type control mice (Figure 3-3J), while alanine was significantly elevated at days 30 and 60 relative to wild type mice (peak at day 30: 497.2 ± 59.8μM vs. 293.9 ± 21.3μM, p = 0.012) (Figure 3-3K). Glutamate showed no significant differences from wild type mice (Figure 3-3L).

Acutely Elevated Ammonia Is Metabolized by Female but not Male sAAV-Treated Mice

To measure the ability of sAAV-treated mice to metabolize ammonia into urea, sAAV-treated and wild type mice (male and female, n = 5 per gender) were subjected to an acute ammonia challenge by injection with 4 mmol/kg of ^{15}N-labeled ammonium chloride (Figure 3-4A). Plasma samples were taken before (time 0) and at 10, 20, 30, 60, and 90 minutes after injection to measure the plasma ammonia and ureagenesis capacity. In sAAV-treated females (red line), plasma ammonia peaked relative to baseline at 20 minutes (535.4 ± 40.4μM vs. 2471.0 ± 317.4μM; p < 0.01) and subsequently decreased over time, with a trajectory toward baseline levels by 90 minutes after injection (937.0 ± 167.0μM; p = 0.16) (Figure 3-4A, red line). Wild type control female mice had a reduced peak ammonia and a more rapid correction to baseline ammonia levels (blue line). Mice were scored at 15 minutes post-injection to examine for any behavioral abnormalities. Treated females averaged a score of 6 (range: 4-7; 7 being no signs of abnormal behavior, i.e., no

noticeable differences from wild types) with no seizure activity while all wild type mice were scored at 7 (Table 3-1).

The results were strikingly different with the male mice. While all female mice completed the challenge, only 2 treated male mice (orange line) survived until the 90-minute time point; the others perished during the challenge (i.e. seizure activity and death). Ammonia levels in treated males, which were higher than females at time 0, reached greater levels above baseline at 20 minutes ($n = 4$ mice; $3389 \pm 348.2\mu M$; $p < 0.05$) and continued to climb during the challenge without returning towards baseline levels (90 minutes: $n = 2$ mice; $5292.5 \pm 841.5\mu M$) (Figure 3-4A, orange line). Similar to the females, male mice were also scored for behavioral abnormalities at 15 minutes post-injection: treated males scored substantially worse however, averaging only a score of 4 (range: 3-6; $p = 0.067$) (Table 3-1); 2 male mice died shortly after with seizure activity. All wild type males scored either 6 or 7 ($n = 3$ scored 6, $n = 2$ scored 7).

In female mice, concomitant with decreases in plasma ammonia, plasma [^{15}N]-urea increased over time before reaching equilibrium at 30 minutes in wild type (blue line) and 60 minutes in sAAV-treated mice (red line) (Figure 3-4B, $p = 0.29$ at 60 minutes). To compare the maximum ureagenic output, the instantaneous rate of ureagenesis was calculated from the slope of the best-fit curve of percent enrichment at time 0, which subsequently demonstrated that sAAV-treated females have 60.3% of wild type capacity ($0.53 \pm 0.04\%$ enrichment/min vs. $0.88 \pm 0.04\%$ enrichment/min [sAAV-treated vs. wild type, respectively], $p < 0.001$) (Figure 3-4C). Male sAAV-treated mice (orange line) also showed gradual incorporation of $^{15}NH_4Cl$ into urea, though at a significantly reduced rate; [^{15}N]-urea enrichment did not reach equilibrium in these mice (Figure 3-4B, $p < 0.01$ at 60 minutes relative to wild type males [black line]). Males produced [^{15}N]-urea at a reduced instantaneous rate compared to wild types ($0.27 \pm 0.03\%$ enrichment/min vs. $0.86 \pm$

0.08% enrichment/min, respectively, $p < 0.001$), representing 31.4% wild type capacity (Figure 3-4C).

hcoCPS1 Transgene and Protein Expression is Upregulated in sAAV-Treated Mice

To measure the amount of hcoCPS1 transgene expression, sAAV-treated mice (n = 5 per group per gender) were euthanized after 120 days post-injection of AAV8-Cre and sAAVs, and livers were removed for molecular analysis. Total DNA was extracted, and vector copy number was determined (Figure 3-5A). There was no significant difference seen in the amount of 5' and 3' sAAVs as copy number per diploid genome in females (5' [left]: 90.08 ± 37.64, 3' [right]: 78.46 ± 32.57; $p = 0.82$). However, in the male mice, there was near statistical significance in the difference in the amount of 5' and 3' sAAVs (left: 132.48 ± 28.67, right: 62.08 ± 10.76; $p = 0.051$).

Total RNA was isolated and used to generate cDNA for qPCR analysis. Using primers that amplify hcoCPS1 and endogenous *Cps1* mRNA (located on the left sAAV), both AAV8-Cre-only (untreated $Cps1^{-/-}$ [n = 5]: 0.02 ± 0.02 fold (2% of wild type), $p < 0.0001$; black bar) and sAAV-treated $Cps1^{-/-}$ (treated [n = 5]: 0.24 ± 0.07 fold (24% of wild type), $p < 0.001$; red bar) females had reduced total CPS1 mRNA relative to wild type *Cps1* gene expression (blue bar) (Figure 3-5B, left). In male mice, total CPS1 mRNA levels were significantly reduced compared to wild types in both untreated [n = 5; black bar at X-axis] and sAAV-treated [n = 5; red bar] mice (0.0009 ± 0.0005 fold (<1% of wild type) and 0.03 ± 0.008 fold (3% of wild type), respectively; $p < 0.0001$ for both groups) (Figure 3-5B).

Liver tissue was used to assess protein levels. In females, sAAV-treated mice showed reduced but substantial CPS1 protein expression compared to the Cps1 protein of wild type controls by Western blot (41.7% ± 11.5, $p < 0.05$ [n = 5]), and trending towards significantly more

than untreated controls (17.3% ± 4.9, $p = 0.08$ [$n = 5$]) (Figure 3-5C, left); however, CPS1 protein in males was substantially less than wild type Cps1 protein (10.2% ± 3.5, $p < 0.0001$ [$n = 5$]) (Figure 3-5C, right), and lower than untreated controls (27.2% ± 2.3, $p < 0.01$ [$n = 5$]), likely only achieving sAAV-based expression just at the level to provide survival with persistent nitrogen vulnerability. Similar differences between untreated and treated mice are seen in tissue sections stained for CPS1 (red). Particularly in females, treated mice show CPS1 protein broadly distributed in the parenchyma with little or no residual endogenous expression visible in untreated mice (Untreated: 85.0 ± 27.3 CPS1+ cells/field; sAAV-treated: 446.5 ± 92.9 CPS1+ cells/field, $p < 0.01$) (Figure 3-5D, top images). Male sAAV-treated mice also had increased quantities of CPS1+ cells relative to untreated mice (sAAV-treated: 417.4 cells ± 80.1; untreated: 34.0 cells ± 20.8; $p < 0.01$) (Figure 3-5D, top images). An enzymatic functional assay was performed on liver lysates to examine the amount of CPS1 activity in sAAV-treated mice ($n = 5$ per gender per group). Female treated mice analyzed after day 120 showed enzyme function of 31.3 ± 6.6% relative to wild type controls ($p < 0.0001$) (Figure 3-5E, left). In males, treated mice had 15.0 ± 1.6% of wild type activity (Figure 3-5E, right; $p < 0.0001$). Taken together, these results demonstrate that sAAV-derived hcoCPS1 expression leads to substantial gene and protein expression in the livers of treated mice, albeit to different extents in females and males.

Discussion

CPS1 deficiency has two clinical presentations: i) neonatal onset, which is typically severe with high morbidity and mortality, and despite treatment, disease progression is difficult to prevent[104]; and ii) late onset, which has milder symptoms brought on by protein-rich meals, infection, pregnancy and the postpartum period, or other situations of high metabolic demand[105]. Biochemically, neonatal onset CPS1 deficiency results in markedly elevated plasma ammonia, leading to encephalopathy with growth and neurological deficits, along with an increase in plasma glutamine and a decrease of plasma citrulline and arginine[90]. In many cases, unrelenting hyperammonemia results in patient deaths. Orthotopic liver transplantation, while curative[106], is limited due to an inadequate supply of available healthy donor livers and has risks of substantial complications[107]; no other curative treatment currently exists. CarbaGlu©, an FDA-approved treatment for n-acetylglutamate synthase (NAGS) deficiency, has been shown to be effective in treating a small subset of CPS1 patients[108], though this is dependent on the nature of the mutation and is not broadly applicable to patients with complete protein loss. The development of novel and efficacious therapeutics is therefore essential to improve patients' quality of life and prevent the morbidity and mortality that accompany this disorder.

To have clinical benefit for patients afflicted with CPS1 deficiency, an effective therapy would need to maintain plasma ammonia in an acceptable range and resolve or prevent hyperammonemic episodes to avoid repeated neurological injury. However, the development of a gene therapy approach for CPS1 deficiency is challenged not only in part by 1) the large size of the cDNA, and 2), until recently, the lack of a clinically relevant animal model of the disorder, but also the expectation of a need for high-level mitochondrial protein expression based on its abundant quantity in normal hepatocytes[88]. A recent study employed mathematical modeling to

investigate ureagenesis at the level of the individual urea cycle enzymes[60], confirming this expectation. A progressive decline in ureagenesis was predicted using a one compartment model when liver-wide CPS1 activity was reduced below 50%. In contrast, ureagenesis was not predicted to decline until enzyme activity was below 3% for ornithine transcarbamylase, 20% for argininosuccinate synthetase, 3% argininosuccinate lyase, and 0.5% for arginase activity.

While our group redeveloped a constitutive Cps1 knockout murine model[61], we chose to test the AAV vector approach in our recently developed conditional Cps1 knockout mouse[64], avoiding investigating this treatment in mice that perish within the first 24 hours after delivery, are very small (~1 gram in size), and develop hyperammonemia shortly after birth with early intake of milk[61]. Use of the conditional model allowed for proof-of-concept studies avoiding these further model complexities. Recent work from our laboratory developing and characterizing the conditional Cps1 knockout mouse model also had demonstrated both the model's amenability to gene therapy strategies and as a representative model of CPS1 deficiency. The use of an AAV encoding Cre recombinase does introduce a small amount of mouse-to-mouse variability in this model; however, at the dose used here, no appreciable differences were seen in the efficiency of knock out.

While AAV is an efficient gene therapy vehicle, its limited ability to package large DNA sequences with the *cis*-regulatory elements necessary for expression is a significant limitation in its application to certain disorders. To address the large size of the CPS1 cDNA, we took an approach taking advantage of the ability of AAVs to undergo intermolecular concatemerization by developing dual vectors with a region of homology, splitting the large transgene into two separate AAV vectors. However, there is inherent inefficiency of transgene expression by this approach; hepatocytes must be transduced by both vectors, intracellular head-to-head and tail-to-tail

concatemerization can occur, limiting successful reconstitution, and homologous recombination is required. Together these issues would typically be expected to result in expression that is lower than that achieved by single AAV vectors[100,109,110]. While it would likely be more efficacious if a single hcoCPS1 cDNA vector could be made, previous unpublished attempts by our lab to generate single AAV vectors expressing CPS1 were unsuccessful, despite repeated efforts. This is possibly due to excessive shearing and genome truncation caused by the oversized AAV genome; encapsidated oversized DNA tends not to be a pure population of large genomes but rather a heterogeneous mixture of mostly genomes truncated to 5 kb or less in size[111–113].

To address the need for high level expression, utilization of the dual vector approach allowed for incorporation of a large and strong promoter (CAG); together with codon optimization of the human CPS1 cDNA, therapeutically relevant expression levels of successfully recombined genomes to control plasma ammonia were achieved. The successful employment of these approaches has allowed us to overcome these major hurdles and permitted the AAV-based delivery and expression of CPS1, avoiding use of less ideal viral vectors that may have limited clinical translatability[64]. Despite previous reports of limitations in CAG-based vectors, such as transgene silencing, immune response to therapeutic protein, and tumorigenesis, no evidence for these effects were seen, similar to previously published work by others[114].

The studies described herein demonstrate the following results for a dual AAV gene therapy approach for CPS1 deficiency: 1) high doses of sAAV vectors with a strong constitutive promoter can lead to expression of CPS1 and result in long-term survival in both male and female mice; however there is a dependence on n-carglumic acid (NCA) to allosterically activate the enzyme to increase the level of enzyme activity; 2) chronic control of plasma ammonia and glutamine (along with alanine, another intermolecular carrier of nitrogen) is achievable, albeit

better in females; and 3) acute control of elevated ammonia and restoration of high-level ureagenesis is achievable in female mice. Untreated control mice perished early and exhibited many of the circulating amino acid perturbations typical of CPS1 deficiency[90], which were notably reversed or mitigated by sAAV treatment.

However, this approach was met with an unexpected result. While female $Cps1^{-/-}$ mice had near-equal transduction of both the 5'and 3' sAAV vectors and long-term ammonia control with avoidance of marked hyperglutaminemia, similar control was not present in the male mice. In contrast to females, male sAAV-treated mice showed a marked increase in glutamine which remained elevated for most of the duration of the study. Elevated glutamine is a typical presentation in proximal urea cycle disorders, and this result supports the moderately elevated plasma ammonia levels and reduced ureagenesis capacity found in the male mice. NCA with dextrose supplementation was efficacious in contributing to improved nitrogen metabolism; as the active ingredient in CarbaGlu, treatment was found to be effective to further assist in control of plasma ammonia long-term. However, NCA and dextrose alone were not sufficient to extend lifespan in mice that did not receive sAAV treatment (data not shown).

Vector dosing in this study was based on weight and, not unexpectedly, male mice were larger. While the circulating blood volume of male compared to female mice is larger[115], this is not as great as the weight difference between genders; thus, effectively an overall greater number of AAV genomes was administered to male mice. This is reflected in the viral DNA copy number per diploid genome of the 5' sAAV: murine hepatocytes from male mice demonstrated nearly 50% more genomes (Figure 3-5) than hepatocytes from female mice. However, unexpectedly, the number of 3' AAV genomes in male hepatocytes was ~50% of the 5' AAV and was only ~80% of the female 3' AAV genomes per diploid nucleus. This reduced 3' sAAV genome number in

hepatocytes from male mice resulted in less full-length hcoCPS1 cDNA, CPS1 protein, enzymatic activity, and ability to handle an exogenous ammonia challenge. The mechanism responsible for this finding is unclear. As both genders received the same dose per kilogram of sAAVs, and male cells have been demonstrated to be transduced more efficiently[116], male mice were expected to have more robust CPS1 enzymatic activity and to outperform females in the exogenous ammonia challenge and ureagenesis experiments. Stochastic differences in vector copy number and sAAV concatemerization, sexually dimorphic AAV expression, and viral retention[117] may have contributed to the differences seen between male and female mice in terms of mRNA and protein expression, enzyme activity, and tolerance to exogenous ammonia loading. Although previous studies have demonstrated that a doubling of vector dose does not reduce viral transduction[109], it is possible that saturation from the larger number of virions (i.e. greater weight in males and thus a greater number of total virions administered) may occur at differential viral loads for females and males. In addition, to our knowledge only two studies using sAAVs have been conducted in both male and female animals[118,119], raising the possibility of sexually dimorphic responses to sAAV administration, concatemerization, expression, or retention that warrant further investigation.

In this study, we injected mice with $5x10^{14}$ GC/kg/virus, which is higher than other reports for gene therapies. A recent study in nonhuman primates demonstrated vector-related toxicity at a dose of $2x10^{14}$ GC/kg[120], indicating that the high viral load could be a barrier to translation. Despite this, high vector dosing has been used for a clinical trial for Duchenne Muscular Dystrophy ($2x10^{14}$ vg/kg) (NCT03375164) and X-linked Myotubular Myopathy ($3x10^{14}$ vg/kg) (NCT03199469). Though no negative effects have been detected at this dose in our studies, such high vector dosing may pose a barrier in terms of production and cost. However, despite this dose, there was no

evidence of acute toxicity or chronic liver injury in mice used in this study. In addition, we found that in a small cohort of females, a reduced dose of $2x10^{14}$ GC/kg/virus was still effective for long-term survival when supplemented with dextrose/NCA (data not shown). Further vector optimization is required and may be achieved by transitioning to a *trans*-splicing or hybrid approach in contrast to the overlapping one used here, which we pursued first due to encouraging early results. Both alternative strategies warrant further investigation for their potential capacity to reduce the viral load necessary for therapeutic benefit.

In summary, we have shown for the first time that CPS1 deficiency may be treated using a split AAV-based gene therapy approach. This work bridges the gap between previously described pre-clinical efforts and more translatable tools to deliver therapeutic CPS1 protein safely and effectively. To date, no other potentially clinically translatable nucleic acid or protein replacement strategies have been successfully implemented to treat CPS1 deficiency.

Materials and Methods

Animal Care and Mouse Procedures

All mice were kept according to the National Institutes of Health guidelines and all experimental procedures were approved by and conducted according to the guidelines of the Institutional Animal Care and Use Committee. Unless otherwise stated, mice had *ad lib* access to standard chow and water and were maintained on a 12-hour light-dark cycle. *Cps1*$^{flox/flox}$ mice on the C57BL/6 background had been developed as previously described[64] and were used for all of the studies. Genomic DNA was prepared from ear clip by standard methods and genotyping was performed by PCR amplification as previously described[64].

Mice were randomly assigned to either the control or the experimental group. Male and female mice were equally represented throughout the study. For injections, AAV was diluted in sterile pharmaceutical grade 0.9% saline (Medline, Northfield, IL, 5T-NFSF-10011) and injected intravenously by a retro-orbital approach under isoflurane anesthesia. AAV8 TBG-Cre recombinase (University of Pennsylvania Vector Core, Philadelphia, PA) was administered ($2x10^{11}$ GC/mouse, a dose previously demonstrated to result in Cps1 deficiency in this model[64]) simultaneously with the sAAVs. All mice were weighed daily and closely monitored for any signs of deteriorating health. Ill-appearing mice (e.g. disheveled fur, hunched appearance, lethargy) were euthanized at a humane endpoint prior to expiration. Mice receiving n-carglumic acid (NCA)-supplemented water were administered a dose of 200mg/L NCA (Sigma-Aldrich, St. Louis, MO, C4375-10G) with 5% (w/v) dextrose (Sigma-Aldrich, G8270); water was replaced daily for females and every 2-3 days for males (on an as-needed basis). Scheduled blood sampling was obtained from the retro-orbital plexus under isoflurane anesthesia with plasma frozen immediately and stored at -80°C until analysis. Samples of liver were either snap frozen at the time of euthanasia

and stored at -80°C until analyzed or were or prepared for immunohistochemistry as described below.

Molecular Cloning

Full-length codon-optimized human *CPS1* (hcoCPS1) was synthesized by Blue Heron Biotech (Bothell, WA). A 467-bp region encompassing base pairs 1714-2181 of the hcoCPS1 transgene was used as the region of homology between the left and right sAAVs. The size of the overlapping region was chosen based on previous data demonstrating that increasing overlap length does not significantly improve recombination efficiency[121]. Molecular cloning of viral vectors was performed according to standard practices. **5' sAAV**: The viral backbone (p1044, provided by the University of Pennsylvania Vector Core) containing AAV2 ITRs was digested with KpnI and XhoI (all restrictions enzymes purchased from New England Biolabs [Ipswich, MA]); the CAG promoter was digested with KpnI and SalI; hcoCPS1 was then PCR-amplified (cDNA base pairs 1-2181) and subsequently digested with KpnI and SalI. Inserts were ligated with Quick Ligase (New England Biolabs, M2200S) into the backbone at a 3:1 molar ratio and transformed into Stbl3 *E. coli* (Invitrogen, Carlsbad, CA, C737303). **3' sAAV**: The same viral backbone as the 5' sAAV was digested with BamHI; hcoCPS1 was PCR-amplified (cDNA base pairs 1714-4521) and subsequently digested with BglII. hcoCPS1 was ligated and transformed similar to the 5' sAAV. The sequences for all primers used here are listed in Table 3-2. PCR conditions for amplifications using Platinum SuperFi DNA polymerase (Thermo Fisher Scientific, Boston, MA, 12351010) were: 95°C for 30s; 67°C for 30s; 72°C for 90s; repeat for 35 cycles. Both constructs were verified by restriction digest and subsequently with sequencing. Viral

amplification and purification of serotype 8 vectors were completed at the University of Pennsylvania Vector Core.

In Vitro Transduction

HEK 293T and HeLa cells were grown in Dulbecco's modified eagle medium (11885-084) supplemented with 10% fetal bovine serum (10437028), 1% GlutaMAX (35050061; all from Invitrogen), and 0.1mg/mL primocin (Invivogen, San Diego, CA, ant-pm-1). Prior to transduction, all cells were passaged and plated at a density of $5.3x10^4$ cells/cm^2. The following day, cells were transduced with increasing sAAV serotype 8 viral genomes/cell in log increments from 10^2 to 10^5 (DNA from 293T cells) or 10^6 (RNA and protein from HeLa and 293T cells, respectively) in growth media supplemented with 5µg/mL polybrene (Vector Builder, Chicago, Il) and incubated overnight (approximately 16 hours). Virus was removed from cells in the morning following transduction by changing to fresh growth media, and cells were grown one additional day in growth media. Cells were then harvested, and total DNA extracted (Qiagen, Germantown, MD, 69504). PCR amplification was performed with Taq DNA Polymerase (Qiagen, 201443). PCR conditions: 95°C for 30s; 60°C for 30s, 72°C for 60s for 35 cycles. RNA was extracted, cDNA synthesized, and qPCR performed for hcoCPS1 as described below. Protein was extracted and analyzed by western blot as described below.

Immunohistochemistry

Whole livers were collected and analyzed as described previously[64]. Briefly, tissues were prepared using standard procedures by fixing in 10% buffered formalin and storing in 70% ethanol until embedding in paraffin. Blocks were sectioned at 4µm thickness onto glass slides. Sections

were baked at 60°C for 1 hour before being deparaffinized in xylene and rehydrated in serial ethanol washes. Slides were boiled in 10mM sodium citrate pH 6.0 to retrieve antigens before permeabilization in 0.1% Triton X-100. Sections were blocked with 10% Normal Goat Serum and incubated with primary antibodies overnight at 4°C. After washing, secondary antibodies were incubated for 1 hour at RT, followed by washing and mounting with VectaShield containing DAPI (Vector Laboratories, Burlingame, CA, H-1200). Primary antibodies used were: CPS1 (Abcam, Cambridge, MA, ab45956, used at 1:1000); GS (Abcam, ab64613, used at 1:1000). Secondary antibodies used were: goat anti-mouse FITC (against GS primary antibody; Invitrogen, M30101, used at 1:200); goat anti-rabbit AF594 (against CPS1 primary antibody; Invitrogen, A-11012, used at 1:200). Quantitation of CPS1+ cells was performed on random fields of the same size in all mice.

qPCR

qPCR was performed as described[64]. Briefly, total RNA was extracted and used to generate cDNA for the PCR reaction according to the manufacturer's instructions (Roche, Indianapolis, IN, 11828665001 and 4897030001, respectively). qPCR was carried out using BioRad ssoAdvanced Universal SYBRGreen (Hercules, CA, 1725271). Primers used are listed in Table 3-2.

Western Blot

Unfixed frozen liver was homogenized, and soluble protein was isolated in RIPA buffer (ThermoFisher Scientific, 89900) and HALT protease inhibitor (ThermoFisher Scientific, 78430). Protein was quantified using BioRad protein assay dye (BioRad, 5000006). Protein was loaded into a 12% gel (BioRad, 4561045) and transferred to PVDF membranes using the TransBlot Turbo

system according to the manufacturer's instructions (BioRad, 1704156). Membranes were blocked in 5% milk and incubated with primary antibodies overnight at 4°C. Secondary antibodies were incubated for 1 hour at RT before detection with SuperSignal West Pico PLUS (ThermoFisher Scientific, PI34579). Primary antibodies: anti-CPS1 (Abcam, ab45956, used at 1:1000); anti-β-actin (Santa Cruz Biotechnology, Santa Cruz, CA, SC47778, used at 1:1000). Secondary antibody: goat anti-rabbit-HRP (against CPS1 primary; Santa Cruz Biotechnology, SC2004, used at 1:5000). No secondary antibody was used for β-actin as the primary antibody is HRP-conjugated. Semi-quantitation was completed using NIH ImageJ version 1.51, normalizing to its own β-actin band to give a ratio of CPS1:β-actin. The average of 5 mice per group was obtained for comparisons.

Ammonia Assay

Whole blood was collected by retro-orbital bleeding under isoflurane anesthesia into capillary tubes coated with sodium heparin (Spectrum Chemical, New Brunswick, USA, 631-11095) and immediately centrifuged at 2000g for 10 minutes at 4°C. Plasma was collected and stored at -80°C until analysis. Ammonia levels were detected using a colorimetric ammonia assay (Abcam, ab83360) according to the manufacturer's instructions.

Ammonia Challenge & Ureagenesis

Mice were fasted for 3-4 hours at the same time of the day. To simulate a nitrogen challenge, mice were injected by intraperitoneal method with a 4 mmol/kg solution of $^{15}NH_4Cl$ (Cambridge Isotope Laboratories, Andover, MA, NLM-467-1). At 15 minutes after injection, the mice were evaluated behaviorally by scoring from one observer using the scale outlined previously[122]. Blood was collected at the indicated time points after injection. Plasma was isolated

and stored at -80°C until analyzed as described above for the ammonia assay. At each bleed, 5 μL of blood was dispensed in duplicate onto a filter paper card (Perkin Elmer, Waltham, MA, GR2261005) for the ureagenesis assay. ^{15}N-labeled urea enrichment was determined on these samples by gas chromatography-mass spectrometry as previously described[123].

CPS1 Enzyme Function Assay

The activity of CPS1 was determined colorimetrically as previously described[55] by assaying at 37°C in an ornithine transcarbamylase coupled reaction, where carbamoyl phosphate was immediately converted to citrulline.

Amino Acid Analysis

The concentration of amino acids in plasma and liver was determined by high-performance liquid chromatography as previously described[64].

Statistical Analysis

Collected data was analyzed with the Prism8 (GraphPad Software, San Diego, CA) statistical package. Results were expressed as mean ± standard error of the mean (SEM) and p values were determined using one-way ANOVA with Tukey's multiple comparison's test, or unpaired T-test when applicable. Error bars represent SEM. $p < 0.05$ was considered significant.

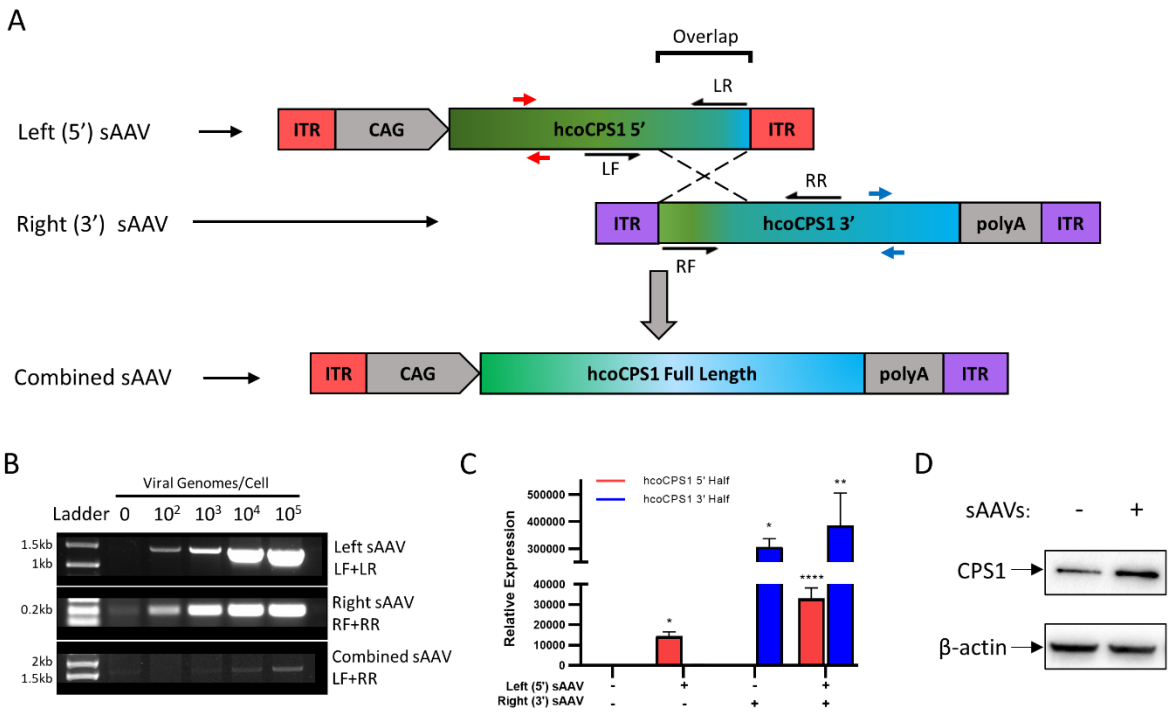

Figure 3-1. *In Vitro* Characterization of sAAVs. **A**) Schematic of overlapping sAAVs. A 467bp overlapping region of homology (overlap) mediates homologous recombination between the 5' (left) and 3' (right) sAAVs, resulting in the full-length combined sAAV containing hcoCPS1 (green-blue rectangles) and removing the intervening viral ITR. **B**) DNA: PCR amplification of left (top) and right (middle) sAAVs and the combined sAAV (bottom) with increasing viral genomes/cell in transduced HEK 293T cells. Amplicons are generated by primers indicated by black half-arrows in A (LF+LR amplify left sAAV; RF+RR amplify right sAAV); combined sAAV product is generated by amplifying with the outer primer of each pair, i.e., primers LF+RR. **C**) RNA: hcoCPS1 mRNA is detectable by qPCR in transduced HeLa cells. Primers used to amplify either half are indicated by red arrows (left sAAV) and blue arrows (right sAAV), and expression was normalized to GAPDH. Data presented are mean ± SEM of triplicate experiments. **D**) Protein: Western blot for CPS1 in HEK 293T cells either non-transduced (- ; left lane) or transduced with both sAAVs (+ ; right lane); β-actin, loading control. (Note: increased density of CPS1 band from sAAV transduced cells.) Abbreviations: CAG, CMV enhancer/chicken β-actin promoter; sAAV, split adeno-associated viral vector; hcoCPS1, human codon-optimized carbamoyl phosphate synthetase 1; HEK, human embryonic kidney; ITR, inverted terminal repeat. *p < 0.05, **p < 0.01, ****p < 0.0001.

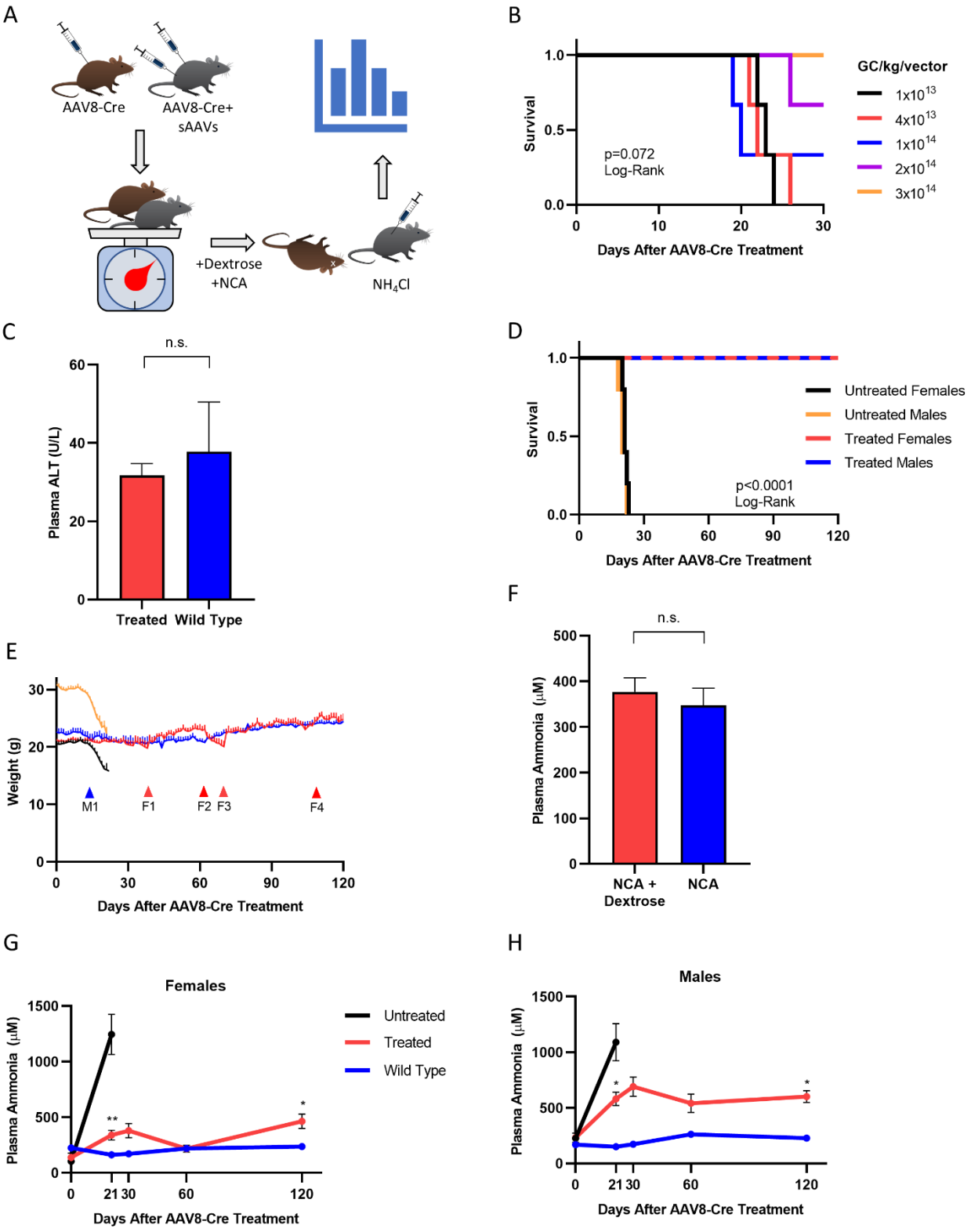

Figure 3-2. sAAVs Promote Lifespan Extension and Weight Maintenance in Mice *In Vivo*. **A**) Workflow of *in vivo* sAAV administration. Adult *Cps1*$^{flox/flox}$ mice were injected with AAV8-Cre alone (mice depicted in brown) or in combination with sAAVs (mice depicted in gray) at time 0

(top left). AAV8-Cre results in hepatic disruption of Cps1 expression resulting in loss of functional protein. All mice were weighed daily to assess general health (bottom left), after which only the surviving sAAV-treated mice (gray) were subjected to an exogenous ammonia challenge after day 120 (bottom right). Mice were subsequently euthanized, and the livers removed for molecular and biochemical analysis (top right). **B**) Dose escalation of sAAVs in female AAV8-Cre-treated *Cps1*$^{flox/flox}$ mice. The minimum dose required to ensure survival to 30 days was determined to be $3x10^{14}$ GC/kg/virus; n = 3 mice per group. **C**) Plasma alanine aminotransferase (ALT) levels in sAAV-treated males (n = 4) are not significantly different from wild type controls (n = 5). **D**) Survival of $5x10^{14}$ GC/kg sAAV-treated (treated [red and blue lines]) mice and AAV8-Cre-only *Cps1*$^{flox/flox}$ (untreated [black and orange]) controls. **E**) Weight maintenance in sAAV-treated mice. AAV8-Cre-only mice (black, orange) rapidly lost weight beginning around day 14 after AAV8-Cre administration, while sAAV-treated mice (red, blue) did not. Red F-series arrows correspond to the red line of treated females; blue M-series arrow corresponds to the blue line of treated males. Red arrows F1 and F3 indicate administration of NCA and dextrose in female sAAV-treated mice (red line); red arrow F2 indicates removal of NCA and dextrose from sAAV-treated females; red arrow F4 indicates removal of dextrose only from NCA water for sAAV-treated female mice; note stability of weight without dextrose. Blue arrow M1 represents addition of NCA and dextrose to male mice. Legend is shared with D. **F**) Plasma ammonia levels are not significantly altered in female sAAV-treated mice when drinking water supplemented with NCA and dextrose or NCA alone (n = 5). **G and H**) Plasma ammonia levels were measured in female (G) and male (H) mice. Legend is shared between G and H; day 21 data points for untreated mice represent values obtained at time of death or euthanasia and are grouped together for clarity. Data represent mean ± SEM with n = 5 mice per group unless otherwise stated; * $p < 0.05$; **$p < 0.01$. Abbreviations: NCA, N-carglumic acid; sAAV, split AAV; SEM, standard error of the mean.

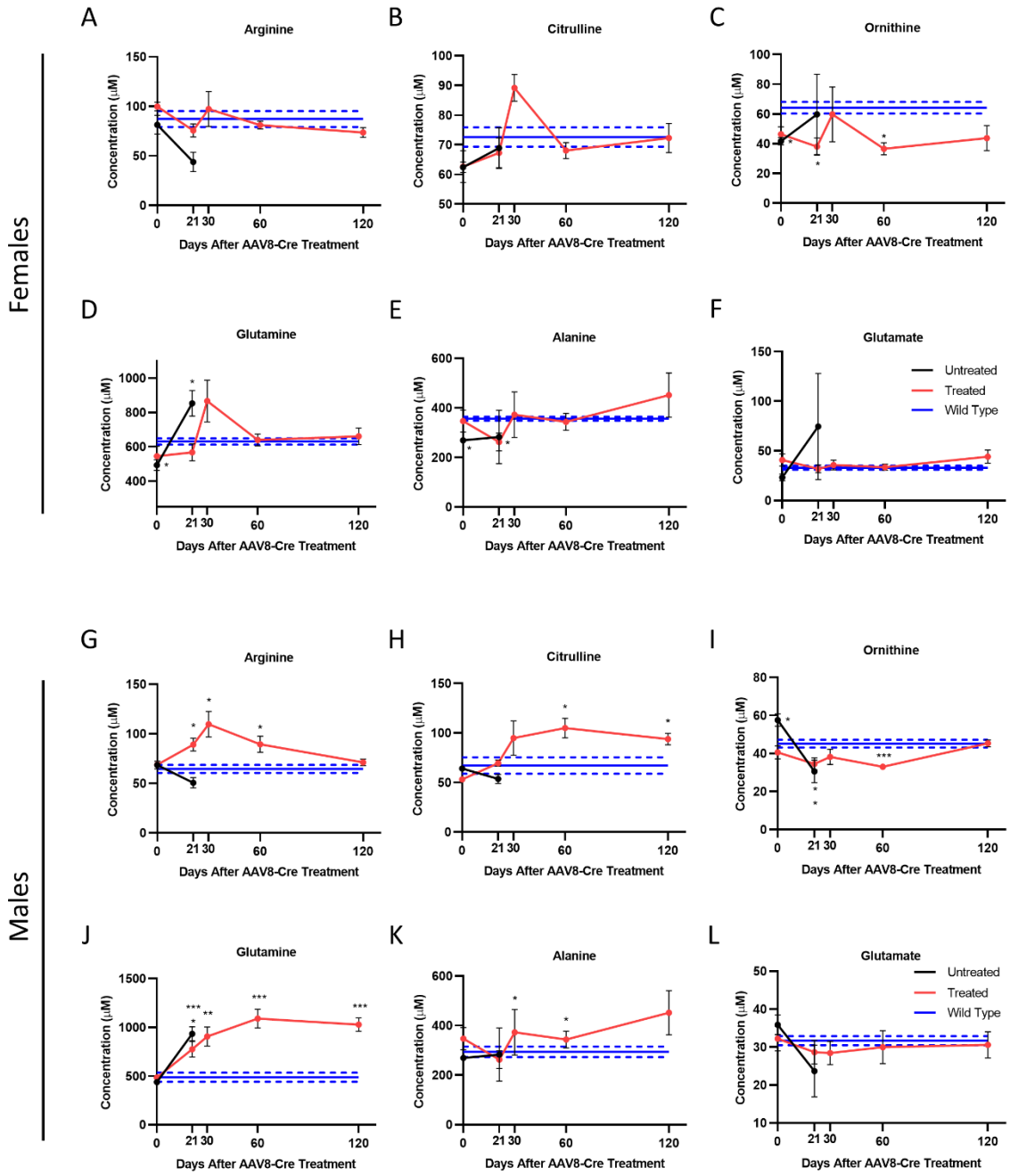

Figure 3-3. sAAV Treatment Improves Some Amino Acid Imbalances in Mice with Cps1 Deficiency. Plasma amino acids show improvement in females (**A**-**F**) and moderate correction in males (**G**-**L**); note sustained elevation of glutamine in sAAV-treated male mice. Data represent mean ± SEM, n = 5 per group except in treated females at day 0, where n = 4. Asterisks denote significant deviation from wild type values, where solid and dashed lines are mean and ± SEM, respectively; *p < 0.05, **p < 0.01, ***p < 0.001.

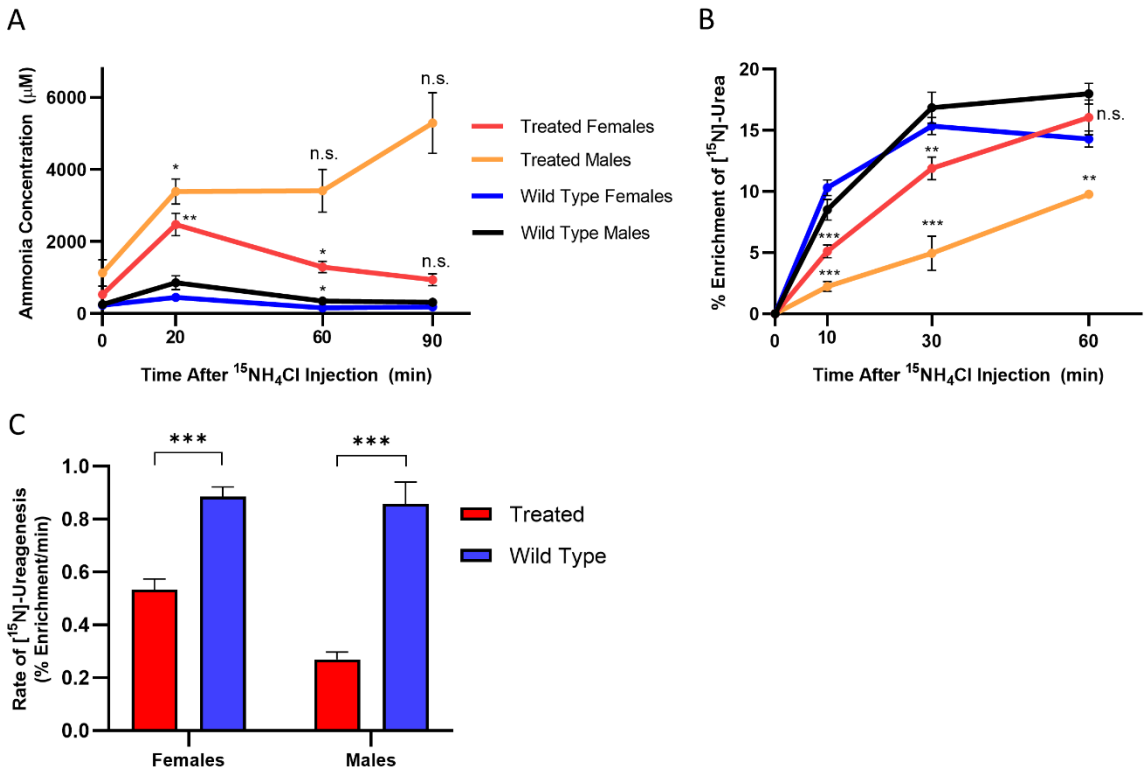

Figure 3-4. Ammonia metabolism after exogenous ammonia loading. **A**) After a marked increase with exogenous administration of $^{15}NH_4Cl$, plasma ammonia levels decrease towards baseline over 90 minutes in female sAAV-treated mice (red line), albeit less rapidly than in wild type mice (blue line). In male sAAV-treated mice plasma ammonia levels do not decline (orange line). Asterisks denote significant deviation from baseline values within a gender. (Treated male mice data at 60 and 90 minutes was n = 2 per time point due to animal deaths, along with large value variation accounts for statistical non-significance.) **B**) ^{15}N-labeled urea is produced in mice treated with $^{15}NH_4Cl$, with enrichment peaking faster in wild type mice (blue, black) than in sAAV-treated mice (red, orange) of both genders. Legend is also shared with A. (A and B: For females at all time points and experimental groups: n = 5 per group. For males: n = 5 at time 0, n = 4 at time 20, and n = 2 at times 60 and 90 in the treated group due to animal deaths from seizure activity; n = 5 at all times for the wild type males.) **C**) Instantaneous rate of ureagenesis in female (n = 5, both groups) and male mice (n = 4 sAAV-treated and n = 5 wild type), based on best-fit curves from B. Data represent mean values ± SEM. Asterisks denote significant deviation from baseline values in the ammonia curves and wild type values in the urea curves; *p < 0.05, **p < 0.01, ***p < 0.001.

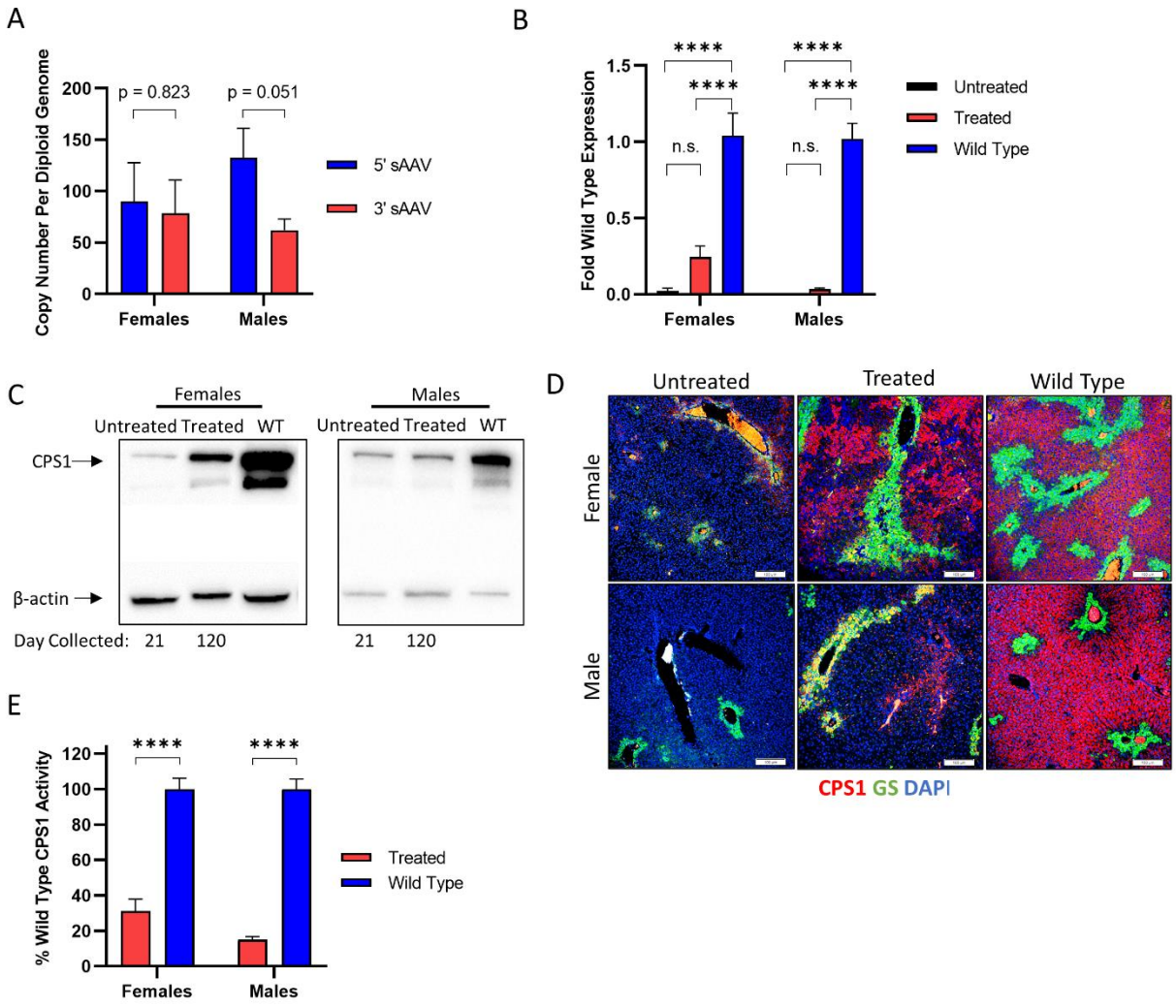

Figure 3-5. Molecular analysis of livers from treated mice. **A**) Vector copy number of both the left (5') and right (3') sAAVs in males (n = 5) and females (n = 5). **B**) Total CPS1 mRNA was measured by qPCR in AAV8-Cre-only (untreated), sAAV-treated (treated), and wild type mice for both females and males (n = 5 per group per gender). **C**) Western blot for CPS1 protein. **D**) Immunofluorescent staining of liver tissue sections for CPS1 (red) and glutamine synthetase (GS) (green); nuclear stained with DAPI (blue). **E**) CPS1 enzyme functional assay on liver tissue lysates in both females and males (n = 5 per group per gender). Western blot and immunofluorescence data are from representative samples; quantitative data represent mean ± SEM. ****p < 0.0001.

Table 3-1. Ammonia challenge behavioral scores. Scores are out of 7; N/A denotes mice that perished prior to scoring.

Females		Males	
Mouse	**Score**	**Mouse**	**Score**
1	6	1	N/A
2	4	2	3
3	7	3	4
4	7	4	3
5	6	5	6

Table 3-2. List of primers

DNA PCR	Sequence	Amplicon Size (bp)
LF	CGGAGCTGAAGTCCATCTTGTCC	1444
LR	CAGCCGCGCATTCACTTCGAT	
RF	ATCGAAGTGAATGCGCGGCTG	194
RR	TCCCACCGAGGAATCTTAGTCACCATATA	
qPCR		
Left sAAV F	GGTTACGCTCTCGATAATACGC	77
Left sAAV R	CCCTCGTTTGTCTGATCATTT	
Right sAAV F	TACCCAACAACCTTGCTGTACCT	135
Right sAAV R	GAGCTTGAGCGACTTTGAGTTCGT	
Total CPS1 F	CTTTGGCCATCCCTCCTCTG	114
Total CPS1 R	TTGGCCATGGTGAGGATCTG	
β-Actin F	CTAAGGCCAACCGTGAAAAG	104
β-Actin R	ACCAGAGGCATACAGGGACA	
GAPDH F	GCTCTCTGCTCCTCCTGTTC	115
GAPDH R	ACGACCAAATCCGTTGACTC	

Chapter 4: Summary and Concluding Remarks

Urea cycle disorders arise from disruptions of function in any of the enzymes or transporter proteins involved in the process, leading to ammonia accumulation-related toxicity. CPS1 deficiency tends to be the most severe of these disorders[2] due to being the first enzyme of the cycle and catalyzing the rate-limiting reaction. Potential new therapies have been developed for the other enzymes of the urea cycle over the past several years[65], however no attempts have been made for CPS1, hindered in part by a lack of appropriate model systems and steep technical challenges. To develop novel potential therapeutics, we established patient-derived iPSC lines which were used in Chapter 2 to investigate how gene editing technologies could be applied to treat the disorder in a cell-based model. In Chapter 3, we used our recently described conditional Cps1 knock out mouse model[64] to establish foundational, proof-of-concept work utilizing a viral gene addition approach.

The Power, Promise, and Limitations of iPSC Technology

Since their invention in 2007[24], iPSCs have been generated in labs the world over to model a broad array of diseases such as autism[124], muscular dystrophy[32], and urea cycle disorders[74]. Their capacity to generate hepatocyte-like cells (HLCs) from patients with metabolic disorders such as CPS1 deficiency make them invaluable tools for studying the native human disease context *in vitro* without the need for primary cells, in addition to supplying an unlimited quantity of cells for transplantation. However, HLCs face important hurdles to translation that must be addressed before their full therapeutic potential can be realized. Arguably the most major hurdle is cell engraftment, studies of which are limited by the widespread use of a mouse model of liver regeneration based on genetic modifications that are not clinically relevant[125,126]. This so-called FRG (Fumarylacetoacetate, Rag2, Il2γ triple knockout) model allows transplanted cells to

repopulate the liver as endogenous hepatocytes die from toxic metabolite buildup upon withdrawal of the drug Nitisinone. This process allows even a small number of engrafted cells to proliferate; however, as the genetic mutations causing this phenotype are rare in humans[127], alternate methods are needed to either improve engraftment or otherwise promote transplanted cell proliferation. One approach has recently been described to mimic the FRG system using a specific inhibitor of fumarylacetoacetate, which would be applicable universally[128]. Another approach utilizes acetaminophen-induced toxicity to kill endogenous cells and allow repopulation by exogenous resistant cells[129], which has the potential to reach the clinic sooner as acetaminophen is already an FDA-approved drug. Another major hurdle to the implementation of HLC transplantation is cell maturity. iPSC-derived HLCs transcriptionally and functionally resemble fetal tissue[130], reducing their capacity to address therapeutic needs[131]. To address this, recent advancements in liver organoids[85,132,133], liver buds[31,134–136], and ectopic artificial livers[137–139] may be used to improve the functional maturity of HLCs and thus their ability to treat diseases. Because of the level of active preclinical research, HLC technology for liver repopulation is expanding rapidly and will likely reach clinical trials in the coming decade.

Beyond the classical deficiency, CPS1 has been implicated in diseases such as cancer[140,141], cardiovascular disease, and obesity (reviewed in Nitzahn and Lipshutz 2020)[142]. Loss of CPS1 expression in hepatocellular carcinomas[143] and gain in lung cancers[141], and subsequent dependence on its expression[144], is intriguing and raises questions about the role of CPS1 in pyrimidine synthesis in these cancers[141,144]. The development of CPS1 deficient iPSCs here may allow for mechanistic and etiological studies on how cancer cells interact with CPS1 to drive and maintain tumorigenesis. In contrast to aberrant expression in cancer, normal expression of a single nucleotide polymorphism (SNP) known as rs1047891 has been implicated in cardiovascular

disease. This SNP encodes an amino acid change of threonine to asparagine that reduces CPS1 activity but does not cause classic CPS1 deficiency[56,145,146]. Reduced CPS1 activity is hypothesized to result in lower levels of substrates for vascular nitric oxide signaling, leading to hypertension under conditions of metabolic stress[145,147]. Rigorous mechanistic investigations have so far been lacking due to the scarcity of cellular models with no CPS1 expression, but the iPSCs established here could be used to investigate nitric oxide signaling in endothelial cells[148] co-cultured with hepatocytes and enterocytes[149] to simulate physiological interactions. Similar studies could be conducted to examine the emerging role of CPS1 in adipocyte function[150,151], which impacts whole-organism metabolism and may hold insights into treating the growing global obesity epidemic. Use of these patient-derived iPSCs as tools to investigate a broader variety of human diseases than once thought highlights their utility and versatility, as well as the need for sustained investigations.

Viruses and Beyond

AAVs were first discovered as contaminants in adenovirus preparations[152,153] and have been in use in clinical trials since the 1990s[154]. Split AAV applications have been described as early as 2000[97], and ours is the latest iteration of them in the pursuit of a virus-mediated gene therapy for CPS1. Our system was successful in providing sufficient exogenous CPS1 expression to prevent mortality and restore urea production in mice, but this proof-of-concept work will require further optimization before reaching patients. A direct comparison of alternative split AAV strategies will be needed to empirically determine which is most suitable for delivering CPS1, as transgene-dependent effects have been observed[98,155]. Additionally, reduction in viral load may be achieved after further investigations of potential small molecules such as vanillin to promote

recombination[156] and bortezomib to increase transduction[157]. The need for recombination could also be circumvented completely by using a single AAV containing the CPS1 transgene and a minimal promoter element. A similar approach has been used to deliver coagulation Factor VIII to hemophilic dogs[158], which was successful despite overfilling the classic 4.7kb AAV genome with >5kb DNA. Preliminary successes in our hands suggest that this approach may also work for CPS1, but high viral loads remain a significant impediment (unpublished).

Despite their relatively safe profile, AAVs, and viruses in general, may not represent the most optimal route for delivering genomic material to hepatocytes to treat CPS1 deficiency. They retain the potential to induce hepatocellular carcinoma[159], and episomal loss over time impacts the durability of AAV-based therapies[51]. The potential to treat a variety of metabolic disorders[160], including urea cycle disorders[161,162], using encapsulated RNA opens the door to a virus-free treatments. Plasmid-based DNA may also be delivered to provide longer-lasting expression[163,164]. Though pilot studies of these approaches in our mouse models have not yet borne fruit, they are at extremely early stages of discovery and hold massive potential to provide a much needed alternative therapy to patients.

Into the Future

CPS1 deficiency has lagged behind in the field of metabolic disorders due to several factors, and the work here has begun to address that disparity. The cell-based approach requires fine tuning, and the virus-based approach has not yet demonstrated efficacy in a stringent neonatal onset disease model. These two separate approaches could be joined to form a combination therapy in which *in utero* HLC transplantation is paired with neonatal split AAV administration to have

both the rapid, high level gene expression of AAVs and the durable, long-term expression of modified, proliferative cells. Recent successes in prenatal hematopoietic stem cell transplantation to treat α-Thalassemia[165] show that this approach is viable. Ongoing work in this area has demonstrated technical feasibility for transplanting hepatic cells to developing fetuses[166]. This combinatorial effort of two distinct modalities could potentially be curative for all patients and deliver truly novel therapeutics to patients. The totality of the work presented here, in which we approached treating CPS1 deficiency using both viral and cellular methods, shows that CPS1 deficiency can be treated successfully and sets the foundation for future work to eventually bring these treatments to the clinic.

References

1. Summar, M.L., Koelker, S., Freedenberg, D., Le Mons, C., Häberle, J., Lee, H.-S., and Kirmse, B. (2013). The incidence of urea cycle disorders. Mol Genet Metab *110*, 179–180.

2. Nettesheim, S., Kölker, S., Karall, D., Häberle, J., Posset, R., Hoffmann, G.F., Heinrich, B., Gleich, F., and Garbade, S.F. (2017). Incidence, disease onset and short-term outcome in urea cycle disorders –cross-border surveillance in Germany, Austria and Switzerland. Orphanet J Rare Dis *12*.

3. Nagata, N., Matsuda, I., and Oyanagi, K. (1991). Estimated frequency of urea cycle enzymopathies in Japan. American Journal of Medical Genetics *39*, 228–229.

4. Uchino, T., Endo, F., and Matsuda, I. (1998). Neurodevelopmental outcome of long-term therapy of urea cycle disorders in Japan. Journal of Inherited Metabolic Disease *21*, 151–159.

5. Marshall, M., Metzenberg, R.L., and Cohen, P.P. (1958). Purification of Carbamyl Phosphate Synthetase from Frog Liver. J. Biol. Chem. *233*, 102–105.

6. McReynolds, J.W., Crowley, B., Mahoney, M.J., and Rosenberg, L.E. (1981). Autosomal recessive inheritance of human mitochondrial carbamyl phosphate synthetase deficiency. Am J Hum Genet *33*, 345–353.

7. Matsumoto, S., Häberle, J., Kido, J., Mitsubuchi, H., Endo, F., and Nakamura, K. (2019). Urea cycle disorders—update. Journal of Human Genetics *64*, 833–847.

8. Enns, G.M., Berry, S.A., Berry, G.T., Rhead, W.J., Brusilow, S.W., and Hamosh, A. (2007). Survival after Treatment with Phenylacetate and Benzoate for Urea-Cycle Disorders. New England Journal of Medicine *356*, 2282–2292.

9. Brusilow, S., Tinker, J., and Batshaw, M.L. (1980). Amino acid acylation: a mechanism of nitrogen excretion in inborn errors of urea synthesis. Science *207*, 659–661.

10. Batshaw, M.L., Brusilow, S., Waber, L., Blom, W., Brubakk, A.M., Burton, B.K., Cann, H.M., Kerr, D., Mamunes, P., Matalon, R., et al. (1982). Treatment of Inborn Errors of Urea Synthesis. New England Journal of Medicine *306*, 1387–1392.

11. Brusilow, SaulW., and Batshaw, MarkL. (1979). ARGININE THERAPY OF ARGININOSUCCINASE DEFICIENCY. The Lancet *313*, 124–127.

12. Batshaw, M., Brusilow, S., and Walser, M. (1975). Treatment of Carbamyl Phosphate Synthetase Deficiency with Keto Analogues of Essential Amino Acids. New England Journal of Medicine *292*, 1085–1090.

13. Hediger, N., Landolt, M.A., Díez-Fernández, C., Huemer, M., and Häberle, J. (2018). The impact of ammonia levels and dialysis on outcome in 202 patients with neonatal onset urea cycle disorders. J Inherit Metab Dis, 1–10.

14. Kalbag, S.S., and Palekar, A.G. (1988). Sodium benzoate inhibits fatty acid oxidation in rat liver: Effect on ammonia levels. Biochemical Medicine and Metabolic Biology *40*, 133–142.

15. Gregus, Z., Fekete, T., Varga, F., and Klaassen, C.D. (1992). Availability of glycine and coenzyme A limits glycine conjugation in vivo. Drug Metab Dispos *20*, 234–240.

16. Batshaw, M.L., MacArthur, R.B., and Tuchman, M. (2001). Alternative pathway therapy for urea cycle disorders: twenty years later. J. Pediatr. *138*, S46-54; discussion S54-55.

17. Zhang, G., Chen, Y., Ju, H., Bei, F., Li, J., Wang, J., Sun, J., and Bu, J. (2017). Carbamoyl phosphate synthetase 1 deficiency diagnosed by whole exome sequencing. J Clin Lab Anal *32*, e22241.

18. Merritt, J.L., Brody, L.L., Pino, G., and Rinaldo, P. (2018). Newborn screening for proximal urea cycle disorders: Current evidence supporting recommendations for newborn screening. Molecular Genetics and Metabolism *124*, 109–113.

19. Largillière, C., Houssin, D., Gottrand, F., Mathey, C., Checoury, A., Alagille, D., and Farriaux, J.-P. (1989). Liver transplantation for ornithine transcarbamylase deficiency in a girl. The Journal of Pediatrics *115*, 415–417.

20. Tuchman, M. (1989). Persistent Acitrullinemia after Liver Transplantation for Carbamylphosphate Synthetase Deficiency. New England Journal of Medicine *320*, 1498–1499.

21. Todo, S., Starzl, T.E., Tzakis, A., Benkov, K.J., Kalousek, F., Saheki, T., Tanikawa, K., and Fenton, W.A. (1992). Orthotopic Liver Transplantation for Urea Cycle Enzyme Deficiency. Hepatology *15*, 419–422.

22. Leonard, J.V., and McKiernan, P.J. (2004). The role of liver transplantation in urea cycle disorders. Mol. Genet. Metab. *81 Suppl 1*, S74-78.

23. Meyburg, J., and Hoffmann, G.F. (2010). Liver, liver cell and stem cell transplantation for the treatment of urea cycle defects. Molecular Genetics and Metabolism *100, Supplement*, S77–S83.

24. Takahashi, K., Tanabe, K., Ohnuki, M., Narita, M., Ichisaka, T., Tomoda, K., and Yamanaka, S. (2007). Induction of Pluripotent Stem Cells from Adult Human Fibroblasts by Defined Factors. Cell *131*, 861–872.

25. Song, Z., Cai, J., Liu, Y., Zhao, D., Yong, J., Duo, S., Song, X., Guo, Y., Zhao, Y., Qin, H., et al. (2009). Efficient generation of hepatocyte-like cells from human induced pluripotent stem cells. Cell Res *19*, 1233–1242.

26. Carpentier, A., Nimgaonkar, I., Chu, V., Xia, Y., Hu, Z., and Liang, T.J. (2016). Hepatic differentiation of human pluripotent stem cells in miniaturized format suitable for high-throughput screen. Stem Cell Res *16*, 640–650.

27. Ang, L.T., Tan, A.K.Y., Autio, M.I., Goh, S.H., Choo, S.H., Lee, K.L., Tan, J., Pan, B., Lee, J.J.H., Lum, J.J., et al. (2018). A Roadmap for Human Liver Differentiation from Pluripotent Stem Cells. Cell Reports *22*, 2190–2205.

28. Gage, B.K., Liu, J.C., Innes, B.T., MacParland, S.A., McGilvray, I.D., Bader, G.D., and Keller, G.M. (2020). Generation of Functional Liver Sinusoidal Endothelial Cells from Human Pluripotent Stem-Cell-Derived Venous Angioblasts. Cell Stem Cell *27*, 254-269.e9.

29. Zhang, R.-R., Koido, M., Tadokoro, T., Ouchi, R., Matsuno, T., Ueno, Y., Sekine, K., Takebe, T., and Taniguchi, H. (2018). Human iPSC-Derived Posterior Gut Progenitors Are Expandable and Capable of Forming Gut and Liver Organoids. Stem Cell Reports *10*, 780–793.

30. Amano, Y., Nishiguchi, A., Matsusaki, M., Iseoka, H., Miyagawa, S., Sawa, Y., Seo, M., Yamaguchi, T., and Akashi, M. (2016). Development of vascularized iPSC derived 3D-cardiomyocyte tissues by filtration Layer-by-Layer technique and their application for pharmaceutical assays. Acta Biomaterialia *33*, 110–121.

31. Ayabe, H., Anada, T., Kamoya, T., Sato, T., Kimura, M., Yoshizawa, E., Kikuchi, S., Ueno, Y., Sekine, K., Camp, J.G., et al. (2018). Optimal Hypoxia Regulates Human iPSC-Derived Liver Bud Differentiation through Intercellular TGFB Signaling. Stem Cell Reports *11*, 306–316.

32. Young, C.S., Hicks, M.R., Ermolova, N.V., Nakano, H., Jan, M., Younesi, S., Karumbayaram, S., Kumagai-Cresse, C., Wang, D., Zack, J.A., et al. (2016). A single CRISPR-Cas9 deletion strategy that targets the majority of DMD patients restores dystrophin function in hiPSC-derived muscle cells. Cell Stem Cell *18*, 533–540.

33. Urnov, F.D., Rebar, E.J., Holmes, M.C., Zhang, H.S., and Gregory, P.D. (2010). Genome editing with engineered zinc finger nucleases. Nature Reviews Genetics *11*, 636–646.

34. Christian, M., Cermak, T., Doyle, E.L., Schmidt, C., Zhang, F., Hummel, A., Bogdanove, A.J., and Voytas, D.F. (2010). Targeting DNA Double-Strand Breaks with TAL Effector Nucleases. Genetics *186*, 757–761.

35. Mahfouz, M.M., Piatek, A., and Stewart, C.N. (2014). Genome engineering via TALENs and CRISPR/Cas9 systems: challenges and perspectives. Plant Biotechnology Journal *12*, 1006–1014.

36. Cong, L., Ran, F.A., Cox, D., Lin, S., Barretto, R., Habib, N., Hsu, P.D., Wu, X., Jiang, W., Marraffini, L.A., et al. (2013). Multiplex Genome Engineering Using CRISPR/Cas Systems. Science *339*, 819–823.

37. Jinek, M., Chylinski, K., Fonfara, I., Hauer, M., Doudna, J.A., and Charpentier, E. (2012). A Programmable Dual-RNA–Guided DNA Endonuclease in Adaptive Bacterial Immunity. Science *337*, 816–821.

38. Martin, R.M., Ikeda, K., Cromer, M.K., Uchida, N., Nishimura, T., Romano, R., Tong, A.J., Lemgart, V.T., Camarena, J., Pavel-Dinu, M., et al. (2019). Highly Efficient and Marker-free

Genome Editing of Human Pluripotent Stem Cells by CRISPR-Cas9 RNP and AAV6 Donor-Mediated Homologous Recombination. Cell Stem Cell *24*, 821-828.e5.

39. Ran, F.A., Hsu, P.D., Wright, J., Agarwala, V., Scott, D.A., and Zhang, F. (2013). Genome engineering using the CRISPR-Cas9 system. Nat Protoc *8*, 2281–2308.

40. Nagamoto, Y., Takayama, K., Tashiro, K., Tateno, C., Sakurai, F., Tachibana, M., Kawabata, K., Ikeda, K., Tanaka, Y., and Mizuguchi, H. (2015). Efficient Engraftment of Human Induced Pluripotent Stem Cell-Derived Hepatocyte-Like Cells in uPA/SCID Mice by Overexpression of FNK, a Bcl-xLMutant Gene. Cell Transplant *24*, 1127–1138.

41. Zhu, S., Rezvani, M., Harbell, J., Mattis, A.N., Wolfe, A.R., Benet, L.Z., Willenbring, H., and Ding, S. (2014). Mouse liver repopulation with hepatocytes generated from human fibroblasts. Nature *508*, 93–97.

42. Asgari, S., Moslem, M., Bagheri-Lankarani, K., Pournasr, B., Miryounesi, M., and Baharvand, H. (2013). Differentiation and Transplantation of Human Induced Pluripotent Stem Cell-derived Hepatocyte-like Cells. Stem Cell Rev and Rep *9*, 493–504.

43. Debnath, T., Mallarpu, C.S., and Chelluri, L.K. (2020). Development of Bioengineered Organ Using Biological Acellular Rat Liver Scaffold and Hepatocytes. Organogenesis *16*, 61–72.

44. Hacein-Bey-Abina, S., Hauer, J., Lim, A., Picard, C., Wang, G.P., Berry, C.C., Martinache, C., Rieux-Laucat, F., Latour, S., Belohradsky, B.H., et al. (2010). Efficacy of Gene Therapy for X-Linked Severe Combined Immunodeficiency. N Engl J Med *363*, 355–364.

45. Brunetti-Pierri, N., Palmer, D.J., Beaudet, A.L., Carey, K.D., Finegold, M., and Ng, P. (2004). Acute Toxicity After High-Dose Systemic Injection of Helper-Dependent Adenoviral Vectors into Nonhuman Primates. Human Gene Therapy *15*, 35–46.

46. Raper, S.E., Chirmule, N., Lee, F.S., Wivel, N.A., Bagg, A., Gao, G., Wilson, J.M., and Batshaw, M.L. (2003). Fatal systemic inflammatory response syndrome in a ornithine transcarbamylase deficient patient following adenoviral gene transfer. Molecular Genetics and Metabolism *80*, 148–158.

47. Tasfaout, H., Lionello, V.M., Kretz, C., Koebel, P., Messaddeq, N., Bitz, D., Laporte, J., and Cowling, B.S. (2018). Single Intramuscular Injection of AAV-shRNA Reduces DNM2 and Prevents Myotubular Myopathy in Mice. Molecular Therapy *26*, 1082–1092.

48. Fuller-Carter, P.I., Basiri, H., Harvey, A.R., and Carvalho, L.S. (2020). Focused Update on AAV-Based Gene Therapy Clinical Trials for Inherited Retinal Degeneration. BioDrugs *34*, 763–781.

49. Colella, P., Ronzitti, G., and Mingozzi, F. (2018). Emerging Issues in AAV-Mediated In Vivo Gene Therapy. Molecular Therapy - Methods & Clinical Development *8*, 87–104.

50. Chandler, R.J., and Venditti, C.P. (2012). Pre-clinical efficacy and dosing of an AAV8 vector expressing human methylmalonyl-CoA mutase in a murine model of methylmalonic acidemia (MMA). Molecular Genetics and Metabolism *107*, 617–619.

51. Lee, E.K., Hu, C., Bhargava, R., Rozengurt, N., Stout, D., Grody, W.W., Cederbaum, S.D., and Lipshutz, G.S. (2012). Long-term Survival of the Juvenile Lethal Arginase-deficient Mouse With AAV Gene Therapy. Molecular Therapy *20*, 1844–1851.

52. Wang, L., Morizono, H., Lin, J., Bell, P., Jones, D., McMenamin, D., Yu, H., Batshaw, M.L., and Wilson, J.M. (2012). Preclinical evaluation of a clinical candidate AAV8 vector for ornithine transcarbamylase (OTC) deficiency reveals functional enzyme from each persisting vector genome. Molecular Genetics and Metabolism *105*, 203–211.

53. Yefimenko, I., Fresquet, V., Marco-Marín, C., Rubio, V., and Cervera, J. (2005). Understanding Carbamoyl Phosphate Synthetase Deficiency: Impact of Clinical Mutations on Enzyme Functionality. Journal of Molecular Biology *349*, 127–141.

54. Pekkala, S., Martínez, A.I., Barcelona, B., Yefimenko, I., Finckh, U., Rubio, V., and Cervera, J. (2010). Understanding carbamoyl-phosphate synthetase I (CPS1) deficiency by using expression studies and structure-based analysis. Hum. Mutat. *31*, 801–808.

55. Díez-Fernández, C., Martínez, A.I., Pekkala, S., Barcelona, B., Pérez-Arellano, I., Guadalajara, A.M., Summar, M., Cervera, J., and Rubio, V. (2013). Molecular Characterization of Carbamoyl-Phosphate Synthetase (CPS1) Deficiency Using Human Recombinant CPS1 as a Key Tool. Human Mutation *34*, 1149–1159.

56. Ahuja, V., and Powers-Lee, S.G. (2008). Human carbamoyl-phosphate synthetase: Insight into N-acetylglutamate interaction and the functional effects of a common single nucleotide polymorphism. Journal of Inherited Metabolic Disease *31*, 481–491.

57. Wang, Y., Chang, L., Zhai, J., Wu, Q., Wang, D., and Wang, Y. (2017). Generation of carbamoyl phosphate synthetase 1 reporter cell lines for the assessment of ammonia metabolism. J. Cell. Mol. Med. *21*, 3214–3223.

58. Eeds, A.M., Mortlock, D., Wade-Martins, R., and Summar, M.L. (2007). Assessing the Functional Characteristics of Synonymous and Nonsynonymous Mutation Candidates by Use of Large DNA Constructs. The American Journal of Human Genetics *80*, 740–750.

59. Yougo, H., Takako, U., Masaki, T., Endo, F., Masataka, M., and Matsuda, I. (1991). Cloning and sequence of a cDNA encoding human carbamyl phosphate synthetase I: molecular analysis of hyperammonemia. Gene *107*, 335–340.

60. Kok, C.Y., Cunningham, S.C., Kuchel, P.W., and Alexander, I.E. (2019). Insights into Gene Therapy for Urea Cycle Defects by Mathematical Modeling. Human Gene Therapy *30*, 1385–1394.

61. Khoja, S., Nitzahn, M., Truong, B., Lambert, J., Willis, B., Allegri, G., Rüfenacht, V., Häberle, J., and Lipshutz, G.S. (2019). A constitutive knockout of murine carbamoyl phosphate

synthetase 1 results in death with marked hyperglutaminemia and hyperammonemia. Journal of Inherited Metabolic Disease *42*, 1044–1053.

62. Schofield, J.P., Cox, T.M., Caskey, C.T., and Wakamiya, M. (1999). Mice deficient in the urea-cycle enzyme, carbamoyl phosphate synthetase i, die during the early neonatal period from hyperammonemia. Hepatology *29*, 181–185.

63. Deignan, J.L., Cederbaum, S.D., and Grody, W.W. (2008). Contrasting Features of Urea Cycle Disorders in Human Patients and Knockout Mouse Models. Mol Genet Metab *93*, 7–14.

64. Khoja, S., Nitzahn, M., Hermann, K., Truong, B., Borzone, R., Willis, B., Rudd, M., Palmer, D.J., Ng, P., Brunetti-Pierri, N., et al. (2018). Conditional disruption of hepatic carbamoyl phosphate synthetase 1 in mice results in hyperammonemia without orotic aciduria and can be corrected by liver-directed gene therapy. Molecular Genetics and Metabolism *124*, 243–253.

65. Baruteau, J., Perocheau, D.P., Hanley, J., Lorvellec, M., Rocha-Ferreira, E., Karda, R., Ng, J., Suff, N., Diaz, J.A., Rahim, A.A., et al. (2018). Argininosuccinic aciduria fosters neuronal nitrosative stress reversed by Asl gene transfer. Nature Communications *9*, 3505.

66. Ye, X., Whiteman, B., Jerebtsova, M., and Batshaw, M.L. (2000). Correction of argininosuccinate synthetase (AS) deficiency in a murine model of citrullinemia with recombinant adenovirus carrying human AS cDNA. Gene Therapy *7*, 1777–1782.

67. McCarron, A., Donnelley, M., McIntyre, C., and Parsons, D. (2016). Challenges of up-scaling lentivirus production and processing. Journal of Biotechnology *240*, 23–30.

68. Muraca, M., Gerunda, G., Neri, D., Vilei, M.-T., Granato, A., Feltracco, P., Meroni, M., Giron, G., and Burlina, A.B. (2002). Hepatocyte transplantation as a treatment for glycogen storage disease type 1a. Lancet *359*, 317–318.

69. Stéphenne, X., Debray, F.G., Smets, F., Jazouli, N., Sana, G., Tondreau, T., Menten, R., Goffette, P., Boemer, F., Schoos, R., et al. (2012). Hepatocyte transplantation using the domino concept in a child with tetrabiopterin nonresponsive phenylketonuria. Cell Transplant *21*, 2765–2770.

70. Stéphenne, X., Najimi, M., Sibille, C., Nassogne, M.-C., Smets, F., and Sokal, E.M. (2006). Sustained engraftment and tissue enzyme activity after liver cell transplantation for argininosuccinate lyase deficiency. Gastroenterology *130*, 1317–1323.

71. Angarita, S.A.K., Truong, B., Khoja, S., Nitzahn, M., Rajbhandari, A.K., Zhuravka, I., Duarte, S., Lin, M.G., Lam, A.K., Cederbaum, S.D., et al. (2018). Human hepatocyte transplantation corrects the inherited metabolic liver disorder arginase deficiency in mice. Molecular Genetics and Metabolism *124*, 114–123.

72. Takayama, K., Akita, N., Mimura, N., Akahira, R., Taniguchi, Y., Ikeda, M., Sakurai, F., Ohara, O., Morio, T., Sekiguchi, K., et al. (2017). Generation of safe and therapeutically effective human induced pluripotent stem cell-derived hepatocyte-like cells for regenerative medicine. Hepatology Communications *1*, 1058–1069.

73. Oceguera-Yanez, F., Kim, S.-I., Matsumoto, T., Tan, G.W., Xiang, L., Hatani, T., Kondo, T., Ikeya, M., Yoshida, Y., Inoue, H., et al. (2016). Engineering the AAVS1 locus for consistent and scalable transgene expression in human iPSCs and their differentiated derivatives. Methods *101*, 43–55.

74. Lee, P.C., Truong, B., Vega-Crespo, A., Gilmore, W.B., Hermann, K., Angarita, S.A., Tang, J.K., Chang, K.M., Wininger, A.E., Lam, A.K., et al. (2016). Restoring Ureagenesis in Hepatocytes by CRISPR/Cas9-mediated Genomic Addition to Arginase-deficient Induced Pluripotent Stem Cells. Mol Ther Nucleic Acids *5*, e394.

75. Truong, B. (2019). Human Induced Pluripotent Stem Cell- and mRNA-based Gene Therapy Strategies for Treatment of Arginase Deficiency.

76. Greenberg, M.V.C., and Bourc'his, D. (2019). The diverse roles of DNA methylation in mammalian development and disease. Nature Reviews Molecular Cell Biology *20*, 590–607.

77. Reizel, Y., Sabag, O., Skversky, Y., Spiro, A., Steinberg, B., Bernstein, D., Wang, A., Kieckhaefer, J., Li, C., Pikarsky, E., et al. (2018). Postnatal DNA demethylation and its role in tissue maturation. Nature Communications *9*, 2040.

78. Xu, C.S., and Chang, C.F. (2008). Expression profiles of the genes associated with metabolism and transport of amino acids and their derivatives in rat liver regeneration. Amino Acids *34*, 91–102.

79. Klatt, D., Cheng, E., Hoffmann, D., Santilli, G., Thrasher, A.J., Brendel, C., and Schambach, A. (2020). Differential Transgene Silencing of Myeloid-Specific Promoters in the AAVS1 Safe Harbor Locus of Induced Pluripotent Stem Cell-Derived Myeloid Cells. Hum Gene Ther *31*, 199–210.

80. Lombardo, A., Cesana, D., Genovese, P., Di Stefano, B., Provasi, E., Colombo, D.F., Neri, M., Magnani, Z., Cantore, A., Lo Riso, P., et al. (2011). Site-specific integration and tailoring of cassette design for sustainable gene transfer. Nat Methods *8*, 861–869.

81. Ordovás, L., Boon, R., Pistoni, M., Chen, Y., Wolfs, E., Guo, W., Sambathkumar, R., Bobis-Wozowicz, S., Helsen, N., Vanhove, J., et al. (2015). Efficient Recombinase-Mediated Cassette Exchange in hPSCs to Study the Hepatocyte Lineage Reveals AAVS1 Locus-Mediated Transgene Inhibition. Stem Cell Reports *5*, 918–931.

82. Wang, Y., Liang, P., Lan, F., Wu, H., Lisowski, L., Gu, M., Hu, S., Kay, M.A., Urnov, F.D., Shinnawi, R., et al. (2014). Genome Editing of Isogenic Human Induced Pluripotent Stem Cells Recapitulates Long QT Phenotype for Drug Testing. Journal of the American College of Cardiology *64*, 451.

83. Spinelli, J.B., Yoon, H., Ringel, A.E., Jeanfavre, S., Clish, C.B., and Haigis, M.C. (2017). Metabolic recycling of ammonia via glutamate dehydrogenase supports breast cancer biomass. Science *358*, 941–946.

84. Finckh, U., Kohlschütter, A., Schäfer, H., Sperhake, K., Colombo, J.-P., and Gal, A. (1998). Prenatal diagnosis of carbamoyl phosphate synthetase I deficiency by identification of a missense mutation in CPS1. Hum. Mutat. *12*, 206–211.

85. Pettinato, G., Lehoux, S., Ramanathan, R., Salem, M.M., He, L.-X., Muse, O., Flaumenhaft, R., Thompson, M.T., Rouse, E.A., Cummings, R.D., et al. (2019). Generation of fully functional hepatocyte-like organoids from human induced pluripotent stem cells mixed with Endothelial Cells. Scientific Reports *9*, 8920.

86. Cascales-Campos, P.A., Ferreras, D., Alconchel, F., Febrero, B., Royo-Villanova, M., Martínez, M., Rodríguez, J.M., Fernández-Hernández, J.Á., Ríos, A., Pons, J.A., et al. (2020). Controlled donation after circulatory death up to 80 years for liver transplantation: Pushing the limit again. American Journal of Transplantation *20*, 204–212.

87. Nitzahn, M., Allegri, G., Khoja, S., Truong, B., Makris, G., Häberle, J., and Lipshutz, G.S. (2020). Split AAV-Mediated Gene Therapy Restores Ureagenesis in a Murine Model of Carbamoyl Phosphate Synthetase 1 Deficiency. Molecular Therapy *28*, 1717–1730.

88. Clarke, S. (1976). A major polypeptide component of rat liver mitochondria: carbamyl phosphate synthetase. J. Biol. Chem. *251*, 950–961.

89. Shi, D., Caldovic, L., and Tuchman, M. (2018). Sources and Fates of Carbamyl Phosphate: A Labile Energy-Rich Molecule with Multiple Facets. Biology (Basel) *7*, 34.

90. Díez-Fernández, C., and Häberle, J. (2017). Targeting CPS1 in the treatment of Carbamoyl phosphate synthetase 1 (CPS1) deficiency, a urea cycle disorder. Expert Opinion on Therapeutic Targets *21*, 391–399.

91. Srinivasan, R.C., Zabulica, M., Hammarstedt, C., Wu, T., Gramignoli, R., Kannisto, K., Ellis, E., Karadagi, A., Fingerhut, R., Allegri, G., et al. (2019). A liver-humanized mouse model of carbamoyl phosphate synthetase 1-deficiency. Journal of Inherited Metabolic Disease *42*, 1054–1063.

92. Smith, D.D., and Campbell, J.W. (1988). Distribution of glutamine synthetase and carbamoyl-phosphate synthetase I in vertebrate liver. PNAS *85*, 160–164.

93. Gaasbeek Janzen, J.W., Moorman, A.F., Lamers, W.H., and Charles, R. (1985). Development of the heterogeneous distribution of carbamoyl-phosphate synthetase (ammonia) in rat-liver parenchyma during postnatal development. J Histochem Cytochem. *33*, 1205–1211.

94. Barzel, A., Paulk, N.K., Shi, Y., Huang, Y., Chu, K., Zhang, F., Valdmanis, P.N., Spector, L.P., Porteus, M.H., Gaensler, K.M., et al. (2015). Promoterless gene targeting without nucleases ameliorates haemophilia B in mice. Nature *517*, 360–364.

95. Rothe, M., Modlich, U., and Schambach, A. (2013). Biosafety Challenges for Use of Lentiviral Vectors in Gene Therapy. Current Gene Therapy *13*, 453–468.

96. Chen, Z.Y., He, C.Y., Meuse, L., and Kay, M.A. (2004). Silencing of episomal transgene expression by plasmid bacterial DNA elements in vivo. Gene Therapy *11*, 856.

97. Sun, L., Li, J., and Xiao, X. (2000). Overcoming adeno-associated virus vector size limitation through viral DNA heterodimerization. Nature Medicine; New York *6*, 599–602.

98. Duan, D., Yue, Y., and Engelhardt, J.F. (2001). Expanding AAV Packaging Capacity with Trans-splicing or Overlapping Vectors: A Quantitative Comparison. Molecular Therapy *4*, 383–391.

99. Ghosh, A., Yue, Y., Lai, Y., and Duan, D. (2008). A Hybrid Vector System Expands Adeno-associated Viral Vector Packaging Capacity in a Transgene-independent Manner. Molecular Therapy *16*, 124–130.

100. Maddalena, A., Tornabene, P., Tiberi, P., Minopoli, R., Manfredi, A., Mutarelli, M., Rossi, S., Simonelli, F., Naggert, J.K., Cacchiarelli, D., et al. (2018). Triple Vectors Expand AAV Transfer Capacity in the Retina. Molecular Therapy *26*, 524–541.

101. Sondergaard, P.C., Griffin, D.A., Pozsgai, E.R., Johnson, R.W., Grose, W.E., Heller, K.N., Shontz, K.M., Montgomery, C.L., Liu, J., Clark, K.R., et al. (2015). AAV.Dysferlin Overlap Vectors Restore Function in Dysferlinopathy Animal Models. Ann Clin Transl Neurol *2*, 256–270.

102. Vidal, P., Pagliarani, S., Colella, P., Verdera, H.C., Jauze, L., Gjorgjieva, M., Puzzo, F., Marmier, S., Collaud, F., Sola, M.S., et al. (2018). Rescue of GSDIII Phenotype with Gene Transfer Requires Liver- and Muscle-Targeted GDE Expression. Molecular Therapy *26*, 890–901.

103. Dyka, F.M., Molday, L.L., Chiodo, V., Molday, R.S., and Hauswirth, W.W. (2019). Dual ABCA4-AAV vector treatment reduces pathogenic retinal A2E accumulation in a mouse model of autosomal recessive Stargardt Disease. Human Gene Therapy.

104. Takeoka, M., Soman, T.B., Shih, V.E., Caviness, V.S., and Krishnamoorthy, K.S. (2001). Carbamyl phosphate synthetase 1 deficiency: A destructive encephalopathy. Pediatric Neurology *24*, 193–199.

105. Häberle, J., Shchelochkov, O.A., Wang, J., Katsonis, P., Hall, L., Reiss, S., Eeds, A., Willis, A., Yadav, M., Summar, S., et al. (2011). Molecular Defects in Human Carbamoyl Phosphate Synthetase I: Mutational Spectrum, Diagnostic and Protein Structure Considerations. Hum Mutat *32*, 579–589.

106. Bates, T.R., Lewis, B.D., Burnett, J.R., So, K., Mitchell, A., Delriviere, L., and Jeffrey, G.P. (2011). Late-onset carbamoyl phosphate synthetase 1 deficiency in an adult cured by liver transplantation. Liver Transpl *17*, 1481–1484.

107. Foschi, F.G., Morelli, M.C., Savini, S., Dall'Aglio, A.C., Lanzi, A., Cescon, M., Ercolani, G., Cucchetti, A., Pinna, A.D., and Stefanini, G.F. (2015). Urea cycle disorders: A case report

of a successful treatment with liver transplant and a literature review. World J Gastroenterol *21*, 4063–4068.

108. Shi, D., Zhao, G., Mew, N.A., and Tuchman, M. (2017). Precision medicine in rare disease: Mechanisms of disparate effects of N-carbamyl-L-glutamate on mutant CPS1 enzymes. Mol Genet Metab *120*, 198–206.

109. Trapani, I., Colella, P., Sommella, A., Iodice, C., Cesi, G., de Simone, S., Marrocco, E., Rossi, S., Giunti, M., Palfi, A., et al. (2014). Effective delivery of large genes to the retina by dual AAV vectors. EMBO Mol Med *6*, 194–211.

110. Colella, P., Trapani, I., Cesi, G., Sommella, A., Manfredi, A., Puppo, A., Iodice, C., Rossi, S., Simonelli, F., Giunti, M., et al. (2014). Efficient gene delivery to the cone-enriched pig retina by dual AAV vectors. Gene Ther *21*, 450–456.

111. Dong, B., Nakai, H., and Xiao, W. (2010). Characterization of Genome Integrity for Oversized Recombinant AAV Vector. Molecular Therapy *18*, 87–92.

112. Wang, Y., Ling, C., Song, L., Wang, L., Aslanidi, G.V., Tan, M., Ling, C., and Srivastava, A. (2012). Limitations of Encapsidation of Recombinant Self-Complementary Adeno-Associated Viral Genomes in Different Serotype Capsids and Their Quantitation. Hum Gene Ther Methods *23*, 225–233.

113. Wu, Z., Yang, H., and Colosi, P. (2010). Effect of Genome Size on AAV Vector Packaging. Mol Ther *18*, 80–86.

114. Mochizuki, S., Mizukami, H., Ogura, T., Kure, S., Ichinohe, A., Kojima, K., Matsubara, Y., Kobayahi, E., Okada, T., Hoshika, A., et al. (2004). Long-term correction of hyperphenylalaninemia by AAV-mediated gene transfer leads to behavioral recovery in phenylketonuria mice. Gene Ther *11*, 1081–1086.

115. Sluiter, W., Oomens, L.W.M., Brand, A., and Van Furth, R. (1984). Determination of blood volume in the mouse with 51Chromium-labelled erythrocytes. Journal of Immunological Methods *73*, 221–225.

116. Davidoff, A.M., Ng, C.Y.C., Zhou, J., Spence, Y., and Nathwani, A.C. (2003). Sex significantly influences transduction of murine liver by recombinant adeno-associated viral vectors through an androgen-dependent pathway. Blood *102*, 480–488.

117. Dane, A.P., Cunningham, S.C., Graf, N.S., and Alexander, I.E. (2009). Sexually Dimorphic Patterns of Episomal rAAV Genome Persistence in the Adult Mouse Liver and Correlation With Hepatocellular Proliferation. Molecular Therapy *17*, 1548–1554.

118. Wang, L., Rosenberg, J.B., De, B.P., Ferris, B., Wang, R., Rivella, S., Kaminsky, S.M., and Crystal, R.G. (2012). In vivo gene transfer strategies to achieve partial correction of von Willebrand disease. Hum. Gene Ther. *23*, 576–588.

119. Al-Moyed, H., Cepeda, A.P., Jung, S., Moser, T., Kügler, S., and Reisinger, E. (2019). A dual-AAV approach restores fast exocytosis and partially rescues auditory function in deaf otoferlin knock-out mice. EMBO Molecular Medicine *11*, e9396.

120. Hinderer, C., Katz, N., Buza, E.L., Dyer, C., Goode, T., Bell, P., Richman, L.K., and Wilson, J.M. (2018). Severe Toxicity in Nonhuman Primates and Piglets Following High-Dose Intravenous Administration of an Adeno-Associated Virus Vector Expressing Human SMN. Human Gene Therapy *29*, 285–298.

121. Halbert, C.L., Allen, J.M., and Miller, A.D. (2002). Efficient mouse airway transduction following recombination between AAV vectors carrying parts of a larger gene. Nature Biotechnology *20*, 697.

122. Ye, X., Robinson, M.B., Pabin, C., Quinn, T., Jawad, A., Wilson, J.M., and Batshaw, M.L. (1997). Adenovirus-Mediated in Vivo Gene Transfer Rapidly Protects Ornithine Transcarbamylase-Deficient Mice from an Ammonium Challenge. Pediatric Research *41*, 527–534.

123. Allegri, G., Deplazes, S., Grisch-Chan, H.M., Mathis, D., Fingerhut, R., Häberle, J., and Thöny, B. (2017). A simple dried blood spot-method for in vivo measurement of ureagenesis by gas chromatography–mass spectrometry using stable isotopes. Clinica Chimica Acta *464*, 236–243.

124. Mariani, J., Simonini, M.V., Palejev, D., Tomasini, L., Coppola, G., Szekely, A.M., Horvath, T.L., and Vaccarino, F.M. (2012). Modeling human cortical development in vitro using induced pluripotent stem cells. PNAS *109*, 12770–12775.

125. Zhang, L., Shao, Y., Li, L., Tian, F., Cen, J., Chen, X., Hu, D., Zhou, Y., Xie, W., Zheng, Y., et al. (2016). Efficient liver repopulation of transplanted hepatocyte prevents cirrhosis in a rat model of hereditary tyrosinemia type I. Scientific Reports *6*, srep31460.

126. Overturf, K., Al-Dhalimy, M., Tanguay, R., Brantly, M., Ou, C.-N., Finegold, M., and Grompe, M. (1996). Hepatocytes corrected by gene therapy are selected in vivo in a murine model of hereditary tyrosinaemia type I. Nat Genet *12*, 266–273.

127. St-Louis, M., and Tanguay, R.M. (1997). Mutations in the fumarylacetoacetate hydrolase gene causing hereditary tyrosinemia type I: Overview. Human Mutation *9*, 291–299.

128. Nygaard, S., Barzel, A., Haft, A., Major, A., Finegold, M., Kay, M.A., and Grompe, M. (2016). A universal system to select gene-modified hepatocytes in vivo. Science Translational Medicine *8*, 342ra79-342ra79.

129. Vonada, A., Tiyaboonchai, A., and Grompe, M. (2021). Drug-Mediated Expansion of Transplanted Hepatocytes In Vivo. 24th Annual Meeting of the American Society of Gene & Cell Therapy, Abstract. Molecular Therapy *29(4)*, Supplement 1, 1–427.

130. Baxter, M., Withey, S., Harrison, S., Segeritz, C.-P., Zhang, F., Atkinson-Dell, R., Rowe, C., Gerrard, D.T., Sison-Young, R., Jenkins, R., et al. (2015). Phenotypic and functional

analyses show stem cell-derived hepatocyte-like cells better mimic fetal rather than adult hepatocytes. Journal of Hepatology *62*, 581–589.

131. Möbus, S., Yang, D., Yuan, Q., Lüdtke, T.H.-W., Balakrishnan, A., Sgodda, M., Rani, B., Kispert, A., Araúzo-Bravo, M.J., Vogel, A., et al. (2015). MicroRNA-199a-5p inhibition enhances the liver repopulation ability of human embryonic stem cell-derived hepatic cells. Journal of Hepatology *62*, 101–110.

132. Hu, H., Gehart, H., Artegiani, B., LÖpez-Iglesias, C., Dekkers, F., Basak, O., Es, J. van, Lopes, S.M.C. de S., Begthel, H., Korving, J., et al. (2018). Long-Term Expansion of Functional Mouse and Human Hepatocytes as 3D Organoids. Cell *175*, 1591-1606.e19.

133. Kanebratt, K.P., Janefeldt, A., Peric, A., Jonsson, J., Johansson, L., Hilgendorf, C., and Andersson, T.B. (2018). Development of a primary human hepatocyte spheroid culture model for drug metabolism and disposition studies. Drug Metabolism and Pharmacokinetics *33*, S69.

134. Yanagi, Y., Nakayama, K., Taguchi, T., Enosawa, S., Tamura, T., Yoshimaru, K., Matsuura, T., Hayashida, M., Kohashi, K., Oda, Y., et al. (2017). In vivo and ex vivo methods of growing a liver bud through tissue connection. Scientific Reports *7*, 14085.

135. Koui, Y., Kido, T., Ito, T., Oyama, H., Chen, S.-W., Katou, Y., Shirahige, K., and Miyajima, A. (2017). An In Vitro Human Liver Model by iPSC-Derived Parenchymal and Non-parenchymal Cells. Stem Cell Reports *9*, 490–498.

136. Takebe, T., Sekine, K., Enomura, M., Koike, H., Kimura, M., Ogaeri, T., Zhang, R.-R., Ueno, Y., Zheng, Y.-W., Koike, N., et al. (2013). Vascularized and functional human liver from an iPSC-derived organ bud transplant. Nature *499*, 481–484.

137. Mazza, G., Rombouts, K., Rennie Hall, A., Urbani, L., Vinh Luong, T., Al-Akkad, W., Longato, L., Brown, D., Maghsoudlou, P., Dhillon, A.P., et al. (2015). Decellularized human liver as a natural 3D-scaffold for liver bioengineering and transplantation. Scientific Reports *5*, 13079.

138. Janani, G., Nandi, S.K., and Mandal, B.B. (2018). Functional hepatocyte clusters on bioactive blend silk matrices towards generating bioartificial liver constructs. Acta Biomaterialia *67*, 167–182.

139. Ijima, H., Nakamura, S., Bual, R.P., and Yoshida, K. (2019). Liver-specific extracellular matrix hydrogel promotes liver-specific functions of hepatocytes in vitro and survival of transplanted hepatocytes in vivo. Journal of Bioscience and Bioengineering *128*, 365–372.

140. Liu, T.H., Li, D.C., Gu, C.F., and Ye, S.F. (1989). Carbamyl phosphate synthetase I. A novel marker for gastric carcinoma. Chin. Med. J. *102*, 630–638.

141. Çeliktaş, M., Tanaka, I., Chandra Tripathi, S., Fahrmann, J.F., Aguilar-Bonavides, C., Villalobos, P., Delgado, O., Dhillon, D., Dennison, J.B., Ostrin, E.J., et al. (2017). Role of CPS1 in Cell Growth, Metabolism, and Prognosis in LKB1-Inactivated Lung Adenocarcinoma. J Natl Cancer Inst *109*, 1–9.

142. Nitzahn, M., and Lipshutz, G.S. (2020). CPS1: Looking at an ancient enzyme in a modern light. Molecular Genetics and Metabolism *131*, 289–298.

143. Butler, S.L., Dong, H., Cardona, D., Jia, M., Zheng, R., Zhu, H., Crawford, J.M., and Liu, C. (2008). The antigen for Hep Par 1 antibody is the urea cycle enzyme carbamoyl phosphate synthetase 1. Laboratory Investigation *88*, 78–88.

144. Ma, S.-L., Li, A.-J., Hu, Z.-Y., Shang, F.-S., and Wu, M.-C. (2015). Co-expression of the carbamoyl-phosphate synthase 1 gene and its long non-coding RNA correlates with poor prognosis of patients with intrahepatic cholangiocarcinoma. Molecular Medicine Reports *12*, 7915–7926.

145. Summar, M.L., Hall, L., Christman, B., Barr, F., Smith, H., Kallianpur, A., Brown, N., Yadav, M., Willis, A., Eeds, A., et al. (2004). Environmentally determined genetic expression: clinical correlates with molecular variants of carbamyl phosphate synthetase I. Molecular Genetics and Metabolism *81*, 12–19.

146. Kaluarachchi, D.C., Smith, C.J., Klein, J.M., Murray, J.C., Dagle, J.M., and Ryckman, K.K. (2018). Polymorphisms in urea cycle enzyme genes are associated with persistent pulmonary hypertension of the newborn. Pediatric Research *83*, 142–147.

147. Summar, M.L., Gainer, J.V., Pretorius, M., Malave, H., Harris, S., Hall, L.D., Weisberg, A., Vaughan, D.E., Christman, B.W., and Brown, N.J. (2004). Relationship Between Carbamoyl-Phosphate Synthetase Genotype and Systemic Vascular Function. Hypertension *43*, 186–191.

148. James, D., Nam, H., Seandel, M., Nolan, D., Janovitz, T., Tomishima, M., Studer, L., Lee, G., Lyden, D., Benezra, R., et al. (2010). Expansion and maintenance of human embryonic stem cell–derived endothelial cells by TGFβ inhibition is Id1 dependent. Nature Biotechnology *28*, 161–166.

149. Macedo, M.H., Araújo, F., Martínez, E., Barrias, C., and Sarmento, B. (2018). iPSC-Derived Enterocyte-like Cells for Drug Absorption and Metabolism Studies. Trends in Molecular Medicine *24*, 696–708.

150. Braga, M., Reddy, S.T., Vergnes, L., Pervin, S., Grijalva, V., Stout, D., David, J., Li, X., Tomasian, V., Reid, C.B., et al. (2014). Follistatin promotes adipocyte differentiation, browning, and energy metabolism[S]. Journal of Lipid Research *55*, 375–384.

151. Nohara, K., Shin, Y., Park, N., Jeong, K., He, B., Koike, N., Yoo, S.-H., and Chen, Z. (2015). Ammonia-lowering activities and carbamoyl phosphate synthetase 1 (Cps1) induction mechanism of a natural flavonoid. Nutr Metab (Lond) *12*, 23.

152. Atchison, R.W., Casto, B.C., and Hammon, W.M. (1965). Adenovirus-Associated Defective Virus Particles. Science *149*, 754–755.

153. Hoggan, M.D., Blacklow, N.R., and Rowe, W.P. (1966). Studies of small DNA viruses found in various adenovirus preparations: physical, biological, and immunological characteristics. PNAS *55*, 1467–1474.

154. Flotte, T., Carter, B., Conrad, C., Guggino, W., Reynolds, T., Rosenstein, B., Taylor, G., Walden, S., and Wetzel, R. (1996). A Phase I Study of an Adeno-Associated Virus-CFTR Gene Vector in Adult CF Patients with Mild Lung Disease. Johns Hopkins Children's Center, Baltimore, Maryland. Human Gene Therapy *7*, 1145–1159.

155. Dyka, F.M., Boye, S.L., Chiodo, V.A., Hauswirth, W.W., and Boye, S.E. (2014). Dual Adeno-Associated Virus Vectors Result in Efficient In Vitro and In Vivo Expression of an Oversized Gene, MYO7A. Human Gene Therapy Methods *25*, 166–177.

156. Paulk, N.K., Loza, L.M., Finegold, M.J., and Grompe, M. (2012). AAV-Mediated Gene Targeting Is Significantly Enhanced by Transient Inhibition of Nonhomologous End Joining or the Proteasome In Vivo. Hum Gene Ther *23*, 658–665.

157. Monahan, P.E., Lothrop, C.D., Sun, J., Hirsch, M.L., Kafri, T., Kantor, B., Sarkar, R., Tillson, D.M., Elia, J.R., and Samulski, R.J. (2010). Proteasome Inhibitors Enhance Gene Delivery by AAV Virus Vectors Expressing Large Genomes in Hemophilia Mouse and Dog Models: A Strategy for Broad Clinical Application. Mol Ther *18*, 1907–1916.

158. Nguyen, G.N., Everett, J.K., Kafle, S., Roche, A.M., Raymond, H.E., Leiby, J., Wood, C., Assenmacher, C.-A., Merricks, E.P., Long, C.T., et al. (2021). A long-term study of AAV gene therapy in dogs with hemophilia A identifies clonal expansions of transduced liver cells. Nature Biotechnology *39*, 47–55.

159. Dalwadi, D.A., Torrens, L., Abril-Fornaguera, J., Pinyol, R., Willoughby, C., Posey, J., Llovet, J.M., Lanciault, C., Russell, D.W., Grompe, M., et al. (2021). Liver Injury Increases the Incidence of HCC following AAV Gene Therapy in Mice. Molecular Therapy *29*, 680–690.

160. Witzigmann, D., Kulkarni, J.A., Leung, J., Chen, S., Cullis, P.R., and van der Meel, R. (2020). Lipid nanoparticle technology for therapeutic gene regulation in the liver. Adv Drug Deliv Rev.

161. Truong, B., Allegri, G., Liu, X.-B., Burke, K.E., Zhu, X., Cederbaum, S.D., Häberle, J., Martini, P.G.V., and Lipshutz, G.S. (2019). Lipid nanoparticle-targeted mRNA therapy as a treatment for the inherited metabolic liver disorder arginase deficiency. Proc Natl Acad Sci U S A *116*, 21150–21159.

162. Cao, J., An, D., Galduroz, M., Zhuo, J., Liang, S., Eybye, M., Frassetto, A., Kuroda, E., Funahashi, A., Santana, J., et al. (2019). mRNA Therapy Improves Metabolic and Behavioral Abnormalities in a Murine Model of Citrin Deficiency. Molecular Therapy *27*, 1242–1251.

163. Grisch-Chan, H.M., Schlegel, A., Scherer, T., Allegri, G., Heidelberger, R., Tsikrika, P., Schmeer, M., Schleef, M., Harding, C.O., Häberle, J., et al. (2017). Low-Dose Gene Therapy

for Murine PKU Using Episomal Naked DNA Vectors Expressing PAH from Its Endogenous Liver Promoter. Mol Ther Nucleic Acids *7*, 339–349.

164. Gallego, I., Villate-Beitia, I., Martínez-Navarrete, G., Menéndez, M., López-Méndez, T., Soto-Sánchez, C., Zárate, J., Puras, G., Fernández, E., and Pedraz, J.L. (2019). Non-viral vectors based on cationic niosomes and minicircle DNA technology enhance gene delivery efficiency for biomedical applications in retinal disorders. Nanomedicine: Nanotechnology, Biology and Medicine *17*, 308–318.

165. Witt, R.G., Nguyen, Q.-H.L., and MacKenzie, T.C. (2018). In Utero Hematopoietic Cell Transplantation: Past Clinical Experience and Future Clinical Trials. Curr Stem Cell Rep *4*, 74–80.

166. Mas, V.R., and Maluf, D.G. (2019). In Utero Cell Transplantation as a Tool for Fixing Liver-based Inherited Metabolic Disorders: Early Technical Evidence Supporting Potential Feasibility. Transplantation *103*, 1300–1301.